Manuscript prepared for Atmos. Meas. Tech.
with version 2014/09/16 7.15 Copernicus papers of the LaTeX class copernicus.cls.
Date: 10 February 2017

Comparisons of the Orbiting Carbon Observatory-2 (OCO-2) X_{CO_2} measurements with TCCON

Debra Wunch[1,12], Paul O. Wennberg[1], Gregory Osterman[2,1], Brendan Fisher[2,1], Bret Naylor[2,1], Coleen M. Roehl[1], Christopher O'Dell[3], Lukas Mandrake[2,1], Camille Viatte[1], David W. T. Griffith[4], Nicholas M. Deutscher[4,5], Voltaire A. Velazco[4], Justus Notholt[5], Thorsten Warneke[5], Christof Petri[5], Martine De Maziere[6], Mahesh K. Sha[6], Ralf Sussmann[7], Markus Rettinger[7], David Pollard[8], John Robinson[8], Isamu Morino[9], Osamu Uchino[9], Frank Hase[10], Thomas Blumenstock[10], Matthäus Kiel[10,1], Dietrich G. Feist[11], Sabrina G. Arnold[11], Kimberly Strong[12], Joseph Mendonca[12], Rigel Kivi[13], Pauli Heikkinen[13], Laura Iraci[14], James Podolske[14], Patrick W. Hillyard[14,19], Shuji Kawakami[15], Manvendra K. Dubey[16], Harrison A. Parker[16], Eliezer Sepulveda[17], Omaira E. G. Rodriguez[17], Yao Te[18], Pascal Jeseck[18], Michael R. Gunson[2,1], David Crisp[2,1], and Annmarie Eldering[2,1]

[1]California Institute of Technology, Pasadena, CA, USA
[2]Jet Propulsion Laboratory, Pasadena, CA, USA
[3]Colorado State University, Fort Collins, CO, USA
[4]University of Wollongong, Wollongong, Australia
[5]University of Bremen, Bremen, Germany
[6]Royal Belgian Institute for Space Aeronomy, Brussels, Belgium
[7]Karlsruhe Institute of Technology (KIT), Institute of Meteorology and Climate Research (IMK-IFU), Garmisch-Partenkirchen, Germany
[8]National Institute of Water and Atmospheric Research, Lauder, New Zealand
[9]National Institute for Environmental Studies (NIES), Tsukuba, Japan
[10]Karlsruhe Institute of Technology (KIT), Institute of Meteorology and Climate Research (IMK-ASF), Karlsruhe, Germany
[11]Max Planck Institute for Biogeochemistry, Jena, Germany
[12]University of Toronto, Toronto, Canada
[13]Finnish Meteorological Institute, Sodankylä, Finland
[14]NASA Ames Research Center, Moffett Field, CA, USA
[15]Japan Aerospace Exploration Agency (JAXA), Tsukuba, Japan
[16]Los Alamos National Laboratory, Los Alamos, NM, USA
[17]AEMet, Izaña, Tenerife, Spain
[18]LERMA-IPSL, Sorbonne Universités, UPMC Univ Paris 06, CNRS, Observatoire de Paris, PSL Research University, F-75005, Paris, France
[19]Bay Area Environmental Research Institute, Petaluma, CA

Correspondence to: Debra Wunch (dwunch@gps.caltech.edu; dwunch@atmosp.physics.utoronto.ca)

Abstract. NASA's Orbiting Carbon Observatory-2 (OCO-2) has been measuring carbon dioxide column-averaged dry air mole fractions, X_{CO_2}, in the Earth's atmosphere for ~~almost~~ over two years. In this paper, we describe the comparisons between the first major release of the OCO-2 ~~version 7Br retrievals~~ retrieval algorithm (B7r) and X_{CO_2} ~~estimates~~ from OCO-2's primary ground-based validation network: the Total Carbon Column Observing Network (TCCON). The OCO-2 X_{CO_2} retrievals, after filtering and bias correction, agree well ~~globally with the TCCON for~~ when aggregated around and coincident with TCCON data in nadir, glint, and target ~~observations, with~~ observation modes, with absolute median differences less than ~~0.5~~0.4 ppm and RMS differences ~~typically below~~ less than 1.5 ppm. ~~Target observations over TCCON stations correlate best with the TCCON data ($R^2 = 0.83$) on a global scale. At local scales, the target comparisons reveal residual biases likely~~ After bias correction, residual biases remain that are latitude-dependent, related to surface properties~~and aerosol scattering~~ , and to scattering by aerosols. It is thus crucial to continue measurement comparisons with TCCON to monitor and evaluate the OCO-2 X_{CO_2} data quality throughout its mission.

1 Introduction

~~NASA's~~ The Orbiting Carbon Observatory-2 (OCO-2) is NASA's first Earth-orbiting satellite dedicated to observing atmospheric carbon dioxide (CO_2) to better understand the carbon cycle. The mission's main goal is to measure carbon dioxide with enough precision and accuracy to characterize its sources and sinks on regional scales and to quantify its seasonal and interannual variability (Crisp et al., 2008; Boland et al., 2009; Crisp, 2015). OCO-2 was successfully launched on July 2, 2014 into low-Earth orbit, and ~~measures~~ its grating spectrometers measure near infrared spectra of sunlight reflected off the Earth's surface in three spectral regions (centered at 0.765 µm, 1.61 µm, and 2.06 µm). Carbon dioxide and oxygen (O_2) in the Earth's atmosphere absorb sunlight at well-known wavelengths in the three spectral regions~~observable by OCO-2, and from~~ . By fitting those absorption features using an optimal estimation retrieval algorithm described in detail by O'Dell et al. (2012) and Connor et al. (2008), atmospheric abundances of carbon dioxide and surface pressure ~~, and~~ are retrieved along with other atmospheric and surface properties (e.g., cloud and aerosol optical depth and distribution, water vapor, temperature, and surface reflectance)~~are obtained (O'Dell et al., 2012; Connor et al., 2008)~~.

The main product from the retrieved abundances of carbon dioxide and surface pressure is the column-averaged dry-air mole fraction of CO_2, called X_{CO_2}, which is ~~a useful product~~ the ratio of CO_2 to the dry surface pressure. The X_{CO_2} quantity is useful for carbon cycle science, as it is ~~directly related to~~ used to directly infer surface fluxes of CO_2~~(Yang et al., 2007; Keppel-Aleks et al., 2011)~~, and is relatively insensitive to vertical mixing (Yang et al., 2007; Keppel-Aleks et al., 2011). In the remainder of this paper, a “measurement” refers to the entire process of producing the atmospheric abundances of X_{CO_2}.

OCO-2 measures X_{CO_2} with unprecedented high precision from space (better than 1 ppm, Eldering et al., 2016) (Eldering et al., 2 possesses biases that the OCO-2 team have attempted to characterize and remove (Mandrake et al., 2015; ?)(Mandrake et al., 2015). To validate the OCO-2 measurements, we use the Total Carbon Column Observing Network (TCCON, Wunch et al., 2011a), a comprehensive ground-based validation network that also measures X_{CO_2}. The TCCON instruments are solar-viewing Fourier transform spectrometers, and they measure the same atmospheric quantity as OCO-2, but their measurements are unaffected by surface properties and minimally affected by aerosols. TCCON instruments cannot measure through optically thick clouds.

The OCO-2 satellite has three viewing modes: nadir mode, in which the instrument points straight down at the surface of the Earth, glint mode, in which the instrument points just off the glint spot on the surface, and target mode, in which the observatory is commanded to scan about a particular point on the ground as it passes overhead. The three modes serve different purposes: the nadir and glint mode measurements are normally used for scientific analyses, and the target mode is used primarily as part of the OCO-2 bias correction procedure. All three modes must be independently verified using comparisons with the ground-based TCCON data. This paper will describe the OCO-2 observation modes in §2, how the OCO-2 version 7 algorithm target-mode retrievals compare with the TCCON data in §??3, and how the glint and nadir mode measurements compare with TCCON data in §4.

2 OCO-2 Observation Modes

OCO-2’s nadir and glint measurements observation modes are considered the nominal “science modes” of the OCO-2 measurement scheme. The nadir observations produce useful measurements only over land and near the sub-solar point over tropical oceans. The glint data are often separated into glint over land (“land glint”) and glint over water (“ocean glint”), as the two modes use different surface reflectance models: Lambertian over land (matching the surface model of the nadir observations), and Cox-Munk over water (?)with a Lambertian component over water. Retrievals are performed over a limited latitude range in glint due to concerns about biases introduced by aerosol scattering over the largest optical path lengths; see Fig. 1. The nadir mode data can provide more reliable X_{CO_2} measurements over higher latitudes over land, which is particularly important in the northern hemisphere, where the boreal forest, the a driver of the CO_2 seasonal cycle, extends north of 70°N. Measurements over inland lakes can be successful in ocean glint mode.

OCO-2 has a geographical “near-repeat” after 16 daysor 233 orbits. During each 16-day period, the satellite orbits the earth 233 times, each orbit along a distinct “orbital path”. The OCO-2 orbit is sun-synchronous, with an equator crossing time near local noon (1:36 pm, Crisp, 2015). The original measurement scheme alternated between glint and nadir observations on alternate 16-day ground track repeat cycles. ~~This is not ideal, due~~ Due to the loss of ocean measurements during nadir mode, and the loss of high latitude measurements during glint mode~~. Thus~~, key components of the carbon cycle (e.g., the springtime draw down of CO_2 due to the onset of the northern hemisphere growing season) ~~would be~~ were poorly sampled. ~~The~~ Thus, the observing strategy was ~~optimized~~ changed to improve the coverage of the oceans and high latitude land masses on July 2, 2015 to alternate between glint and nadir modes for each subsequent orbit. The OCO-2 observation scheme was ~~further~~ optimized on November 12, 2015, to assign orbits that are almost entirely over ocean to ~~be always measured~~ always measure in glint mode. This change ~~was made~~ occurred on 72 out of the 233 orbital paths: 15 over the Atlantic and 57 over the Pacific, resulting in higher data throughput ~~because there are now fewer~~ due to the reduction in nadir soundings over ocean. ~~?~~ Crisp et al. (2017) discuss the measurement strategy in detail.

Target mode ~~was designed to assist the OCO-2 science team in evaluating the~~ is designed to evaluate biases in the OCO-2 X_{CO_2} product. The target locations are mostly selected to be coincident with ground validation stations, typically at TCCON sites. During a target-mode maneuver, the OCO-2 satellite rotates from its nominal science mode to point at a selected ground location. This transition takes approximately 5 minutes and rotates the spacecraft's solar panels away from the sun. The spacecraft then scans across the site or "nods" as it passes overhead to sweep across the ground several times (see Fig. 2) over a period of about 4.5 minutes: these dithered measurements comprise the "target-mode data". The spacecraft then transitions out of target mode and back into its nominal science mode over the next 5 minutes. In total, the maneuver takes about 14.5 minutes, and during this time, the spacecraft, traveling at 7.5 $\mathrm{km \cdot s^{-1}}$, has traveled over 6,500 km.

The strength of target mode measurements is that thousands of spectra are obtained in a short period of time over a small region of the world (about 0.2° longitude × 0.2° latitude for the densest measurements~~,~~). For example, in Fig. 2~~)~~, there are 3473 soundings in the region around the Lamont TCCON station. As long as the target location is far from large emissions sources, X_{CO_2} can be assumed constant spatially and temporally within a target ~~measurement~~region, because atmospheric X_{CO_2} is unlikely to change significantly over small geographic regions within 4.5 minutes. However, during the maneuver, many other parameters can change significantly, such as the atmospheric path, the path length of the measurement (the "airmass"), surface reflectivity (albedo), and topography. Any variability in the retrieved X_{CO_2} in the target mode data is considered to be an artifact, and can provide insight into biases caused by the algorithm's treatment of the parameters. With this in mind, the target locations were carefully chosen to span a wide range of latitudes, longitudes, and surface types to challenge the OCO-2 retrieval algorithm and reveal any biases ~~caused by it~~ it causes.

2.1 Target Locations and Selection

There ~~is~~ are a limited number of ground locations that can be targeted because the locations must be pre-programmed into the spacecraft software. For the first year after launch, there were 19 possible target locations. In July 2015, 8 additional targets slots became available, allowing for 27 target locations. At several times, target locations have been changed or replaced. A list of the ground target locations and dates is provided in Table 1, and a map of their locations is in Fig. 3. Individual locations can be targeted by OCO-2 only on specific OCO-2 orbit paths. Only one target location can be assigned to a given orbit path, and only if the OCO-2 ground track for that path is sufficiently close to the ground target location. Thus for each day, there are between one and seven ground target locations to choose from. The spacecraft power systems can handle up to three target-mode maneuvers per day due to the power constraints imposed by rotating the spacecraft solar panels away from the sun. We typically select only one target per day. ~~On 40 occasions, we have targeted two locations on one day; on 3 occasions, we have targeted 3 locations on one day.~~

There are several TCCON stations that are located in regions with ~~spatially varying~~ significant spatial variability in topography or ground cover. For example, the ~~Białystok TCCON station has a nearby forest, the~~ Lauder TCCON station is in the midst of rolling hills, the Wollongong TCCON station is between the ocean and a sharp escarpment, ~~the Darwin TCCON station is near the coast close to sea level,~~ and the Edwards TCCON station is adjacent to a very bright playa, a land surface property previously identified ~~in~~ from the Greenhouse Gases Observing Satellite ~~(GOSAT, Kuze et al., 2009; ?) project~~ (GOSAT, Kuze et al., 2009, 2016) results as challenging for space-borne X_{CO_2} retrievals (Wunch et al., 2011b). With target-mode measurements, the impact that local surface variability has on the X_{CO_2} retrievals becomes apparent.

Other TCCON stations (e.g., Park Falls, Lamont) have relatively uniform surface properties and are reasonably far from anthropogenic CO_2 sources, but the ground cover can vary from season to season. ~~Park Falls is snow-covered in winter, dark green in summer. Lamont is green in spring and brown in winter.~~ The Sodankylä and Eureka sites, located at high northern latitudes, challenge the OCO-2 algorithm at very high solar zenith angles and airmasses, and with snowy scenes. Izaña, Réunion and Ascension, all lower-latitude sites, are located on small islands remote from large land masses, but with significant topography. The Izaña TCCON station (28.3°N) is at 2.37 km altitude, whereas the Réunion (20.9°S, 0.087 km) and Ascension Island (7.9°S, 0.032 km) stations are closer to sea level.

Several TCCON target stations are near or in urban regions with varied topography and emissions sources: Pasadena ~~is in the South Coast Air Basin of California, which contains the city of Los Angeles and is home to 17 million residents. Tsukuba is in a highly urbanized city near Tokyo~~ (pop. ~17 million), Tsukuba (pop. ~228,000)~~. The Paris TCCON station is located 4.5 from the Eiffel Tower in the heart of the city~~, Paris (pop. ~2.24 million), and ~~the Karlsruhe TCCON station is in a smaller, more isolated urban region~~ Karlsruhe (pop. ~300,000)~~surrounded by forest~~.

There are several target locations that are not TCCON stations (Fig. 3, orange stars), and although data from those targets will not be analysed in this paper, the data will help assess biasthe radiometric calibration of the instrument, its ability to measure large urban sources of CO_2, validate its solar-induced fluorescence observations (Frankenberg et al., 2014), and assess its ability to measure vertically-resolved information about CO_2. Railroad Valley is a heavily instrumented radiometric calibration site (Kuze et al., 2011);, and Libya has surface properties that are valuable for radiometric calibration. Shanghai, São Paulo and Mexico City are geographically well-constrained urban regions with significant CO_2 emissions;. Rosemount and Litchfield have instrumentation that will help verify the OCO-2 solar induced fluorescence observations;. Boulder has frequent AirCore CO_2 profile measurements (Karion et al., 2010); Fairbanks is . Fairbanks is the location of a future TCCON station. The Libya location has very specific and consistent surface properties and observations there will improve the radiometric calibration of

The OCO-2 .

2.2 Target Selection

Target spacecraft must be manually commanded to perform a target maneuver. The target locations are selected a day or two in advance, based on the weather forecast, the operational status of the TCCON station (if the target is a TCCON station), the importance of the projected data loss in nadir or glint mode from performing the target-mode operation, and the historical statistics of successful target-mode measurements over that site. The projected data loss depends primarily on whether the nominal mode for that orbit was nadir over land, nadir over ocean, glint over land, or glint over ocean. If the nominal mode is nadir over ocean, little useful data loss occurs, as nadir measurements over ocean are usually too dark in the near infrared for successful retrievals: in this case, the target is almost always selected given a reasonable weather forecast. This has mostly been the case for Réunion Island, which has been targeted regularly from OCO-2 nadir orbits. For the other three cases, there will be some loss of regular science data to accommodate a target-mode operation. In these cases, the historical statistics of acquiring good target-mode data and weather forecasts are weighted more heavily before enabling the target. Often, if the weather forecast is not ideal, no target-mode measurements will be selected.

As of April 30December 31, 2016, 227 264 targets have been selected, 195 observed, 230 of them over TCCON stations(Fig. ??). Of the 195 targets of TCCON stations, about 90% were "successful", in that both OCO-2 data and TCCON data were recorded. This 10% loss was largely due to poor weather forecasts, resulting in completely overcast skies, during which the TCCON station was unable to record any data. There were two instances of unforeseen mechanical failures at TCCON stations. The TCCON data have been analysed for 90% of those targets. Of the 195 targetsrecorded, about 55% remaining 208 targets, about 59% (123) were clear enough to obtain sufficient high-quality (low warn level) OCO-2 data to compare with TCCON data.

3 Target ~~Mode Comparisons to TCCON~~ mode and ~~Residual Bias Assessment~~the OCO-2 bias correction

All current space-based X_{CO_2} measurements have systematic biases. These biases can be caused by uncertainties in the spectroscopy, by limitations in the information content of the measurements ~~and~~ (i.e., the spectra do not contain enough information to resolve multiple independent vertical pieces of information), by uncertainties or oversimplifications in the optical properties of the atmosphere and surface, particularly from low-lying cloud, haze and aerosols, and by uncertainties in the instrument characterization and calibration ~~(e.g., ?Wunch et al., 2011a; Guerlet et al., 2013; Schneising et al., 2012)~~(e.g., Crisp et al., 2017; W Considerable effort is dedicated to creating robust "bias ~~corrections".~~ correction" procedures, and these are detailed in regularly updated documentation available online through the Goddard Data Center (GES-DISC, 2016) and the CO_2 portal (JPL-Caltech, 2016). The current bias correction procedure is described in Mandrake et al. (2015).

There are three key types of biases ~~considered here, and the bias correction addresses them all: the first is any constant scaling factor from the World Meteorological Organization (WMO) trace-gas standard scale (a "constant" bias), the second is~~ addressed by the OCO-2 bias correction procedure: footprint-dependent biases; spurious correlations of the retrieved X_{CO_2} with other retrieval parameters such as the surface pressure retrieval error, signal level, airmass, surface albedo, or retrieval stability (a "parameter-dependent" bias)~~, and the third is any footprint-dependent biases~~; and a scaling factor from the World Meteorological Organization (WMO) trace-gas standard scale (Zhao and Tans, 2006), which we will refer to as a "scaling" bias.

The OCO-2 instrument records 8 spectra simultaneously, each with a slightly different atmospheric path, and hence measures sunlight that has reflected off of a different surface location or "footprint". Footprint-dependent biases are corrected ~~with calibration observations compiled using a special~~ using a subset of OCO-2 data collected ~~while the spectrometer slit is oriented parallel to the ground track and the eight~~ over small areas around the world in which there were at least 100 soundings with low variability, and where all eight footprint measurements resulted in a successful retrieval (Mandrake et al., 2015). Note that there are two footprint-dependent corrections applied to the B7 OCO-2 ~~footprints are geographically coincident (Mandrake et al., 2015). The parameter-dependent biases must be removed before the constant scaling factor can be established, as~~ data: one that is applied as part of the standard bias correction algorithm, and one that was discovered after the generation of the bias correction. This second "residual footprint bias" correction must be applied manually by the ~~parameter-dependent bias correction can impact the magnitude of the constant scaling factor. The procedure by which the OCO-2 data have been bias-corrected is documented in detail by Mandrake et al. (2015) and ? and is briefly described here.~~ data user (Mandrake et al., 2015). In all subsequent analyses in this paper, both footprint dependent biases are removed from the data, unless otherwise specified. In future versions of the OCO-2 algorithm, there will be no residual footprint bias correction required.

The parameter-dependent bias correction uses a genetic algorithm to determine which retrieval parameters account for the largest fraction of the spurious variability found in the estimated X_{CO_2} on large spatial scales (Mandrake et al., 2013, 2015). The algorithm uses several subsets of the OCO-2 data for this task: a "southern hemisphere approximation" which exploits the low spatial and temporal variability of X_{CO_2} in the the southern hemisphere south of 25°S (e.g., Wunch et al., 2011b); a "small area analysis" which exploits the low spatial variability of X_{CO_2} within small regions (0.89° latitude on a single orbit track) and can be applied at all latitudes; and data near coastlines wherein spurious differences in X_{CO_2} between adjacent land and ocean measurements can be clearly diagnosed (Mandrake et al., 2015). A multivariate regression is performed between spurious X_{CO_2} variability and the parameters. The resulting slopes of the regressions allow us to then subtract the predicted bias from the X_{CO_2} values. In the results that follow, the footprint and parameter-dependent biases in the OCO-2 target-mode data have been removed following Mandrake et al. (2015), allowing us to determine the constant scaling factor scaling factor to tie the OCO-2 X_{CO_2} scale to the TCCON scale. The parameter dependent corrections must be removed first, because they can affect the scaling bias if the global mean value of X_{CO_2} at the mean parameter value differs from that of the mean filtered value.

Placing the OCO-2 data on the World Meteorological Organization's (WMO) trace-gas standard scale is crucial to obtaining flux inversions for obtaining accurate flux estimations that are consistent with the state-of-the-art inversions of inversions of the surface in situ CO_2 data, which measurements that are carefully calibrated to the WMO scale (Zhao and Tans, 2006). To achieve this, we compare the The TCCON data are tied to the WMO scale and serve as the link between the calibrated surface in situ measurements and the OCO-2 target mode data with the latest version of the TCCON data (GGG2014, ?), which have been tied measurements.

To tie the TCCON measurements to the WMO trace-gas standard scalethrough comparisons with scale, over 30 profiles of in situ CO_2 profiles from aircraft (Wofsy, 2011; Pan et al., 2010; Singh et al., 2006) and AirCore (Karion et al., 2010), following the methods described by Wunch et al. (2010). have been measured directly overhead of 15 TCCON stations with aircraft carrying carefully calibrated instrumentation (Wofsy, 2011; Pan et al., 2010; Singh et al., 2006) or AirCore (Karion et al., 2010). These profiles, the first of which occurred in 2004, vary in altitude range, depending on the vehicle, and thus must be combined with a priori information about the CO_2 in the highest altitudes of the atmosphere to generate a full vertical profile. These profiles are then integrated, smoothing with the TCCON averaging kernel and a priori profile to compute the best estimate of the "true" X_{CO_2} value. Integrated profiles are compared with the retrieved X_{CO_2} from the TCCON spectra and result in a highly linear relationship which defines a multiplicative bias between the TCCON X_{CO_2} and the best estimate of the "truth". Removing this bias from the TCCON X_{CO_2} ties it to the WMO scale. The details of this method of tying the TCCON X_{CO_2} to the WMO scale are described in Wunch et al. (2010), Washenfelder et al. (2006), Messerschmidt et al. (2011), and in Wunch et al. (2015).

We consider TCCON data to be coincident with the OCO-2 target-mode measurements when they have been recorded within ±30 minutes of the time at which the spacecraft is closest to nadir during the maneuver. If there are fewer than 5 TCCON data points recorded within that time, the window is extended to ±120 minutes, but this is required in only ~~14~~10% of cases. We use the full OCO-2 version ~~7B~~ B7 retrospective data (i.e., ~~7Br~~B7r), available from GES-DISC (2016, http://disc.sci.gsfc.nasa.gov/OCO-2), and manually apply the filters listed in Table 2. ~~These~~

The analyses of the target mode data to develop the scaling bias are completed prior to the generation of "warn levels" and the official filtering schemes, and this scaling bias is applied as part of the bias correction procedure required to generate the "lite" files used commonly by the scientific community. Warn levels determine sets of OCO-2 data with consistent quality data (as defined by the RMS scatter) within an observation mode (Mandrake et al., 2013, 2015). A significant volume of data is required to generate warn levels which is difficult to achieve with the relatively sparse target mode data. Furthermore, individual warn levels in one measurement mode are not necessarily equal in quality to another mode. The target mode filters are consistent with the "warn level 15" scheme described by Mandrake et al. (2015), except that the filter on the surface pressure difference from the prior in the A-band pre-processor is loosened, and we have added an additional outlier filter.

Figure 3 shows the OCO-2 X_{CO_2} target-mode median data comparisons with coincident TCCON data. The best fit lines were computed using a method that accounts for uncertainties in the dependent and independent variables ~~as described by York et al. (2004)~~(York et al., 2004). Panel (a) shows the results prior to applying the parameter-dependent bias correction and has a correlation coefficient of ~~$R^2 = 0.75$~~$R^2 = 0.78$. Panel (b) shows the relationship after the correction has been applied and an improved correlation coefficient (~~$R^2 = 0.83$~~$R^2 = 0.86$). The improvement indicates that the parameter-dependent bias correction is effective at removing spurious variability in the OCO-2 data with respect to TCCON. The slope in panel (b), which has a y-intercept that is forced through 0, is used to derive the ~~constant~~ scaling factor between TCCON and OCO-2 target observations (~~$m = 0.9975 \pm 0.04$~~$m = 0.9977 \pm 0.04$, which represents ~1 ppm) for the time period spanning September 8, 2014 through ~~April 30~~December 31, 2016. The y-intercept is forced through 0 because it is assumed that in the absence of atmospheric CO_2, both OCO-2 and TCCON will measure 0 ppm. The scaling factor derived as part of the Mandrake et al. (2015) bias correction procedure was produced using the data available at the time, which spanned November 2014 through May 2015, and resulted in a similar, but not identical slope of 0.99694 ± 0.00102. This scaling bias difference results in a 0.3 ppm offset between OCO-2 and TCCON X_{CO_2} at 400 ppm, with the standard bias-corrected OCO-2 measurements high. Panel (c) of Fig. 3 shows the relationship between the OCO-2 X_{CO_2} after applying the bias correction, scaling and the residual footprint correction ($m = 1.0007 \pm 0.04$, $R^2 = 0.86$). The residual footprint correction does not impact the slope or R^2 value of the relationship.

The long term time-dependence of the difference between the OCO-2 target-mode data and the coincident TCCON data (ΔX_{CO_2}), after the constant scaling bias is removed, is plotted in Fig. 4. The algorithm, calibration and instrument cause no apparent time-dependent drift in ΔX_{CO_2} nor their errors. Thus, the bias correction is successful at reducing both the parameter-dependent and constant global global scaling biases.

However, the target mode measurements are sensitive enough to point to some residual biases (i.e., those not corrected by the Mandrake et al. (2015) bias correction process) that are currently under investigation by the OCO-2 algorithm, calibration and validation teams. These residual biases are more geographically localized in nature and appear to be related to surface properties, and as such might not be expected to be captured by the standard bias correction, which is designed to minimize globally-relevant biases. The residual biases seem to fall into two classes: biases in high southern latitude ocean glint data (§**??**), and biases caused by the surface properties at a target location (§3.1).

3.1 Surface Properties

Biases Related to Surface Properties]Southern hemisphere winter glint measurements over waterIn the southern hemisphere winter, there is a significant high bias in the retrieved from the OCO-2 ocean glint data. There were three target-mode measurements recorded in the southern hemisphere during that time: two points over Wollongong, and a third point over Réunion recorded during late July/early August 2015 (Fig. 4). Figure **??** illustrates this problem by showing the divergence of the latitude gradients of the OCO-2 in all viewing modes and the TCCON during August 2015 and the agreement in October 2015. Appendix Fig. A0 panels (r) and (s) also show this problem as a function of time. This bias does not impact the overall one-to-one line within the uncertainty but does impact the latitudinal gradients (and hence fluxes) inferred by the OCO-2 data. While the cause of the bias in the southern winter is currently unclear, there is a working hypothesis related to the OCO-2 algorithm's misrepresentation of stratospheric aerosols, exacerbated by the eruption of Mount Calbuco in Chile on April 22, 2015 (Romero et al., 2016). This is described in detail in ?.

3.1 Surface Properties

Biases Related to Surface Properties Site-dependent differences from the one-to-one plot in Fig. 3(b), shown in Fig. 5, reveal significant location-dependent biases. Any differences with magnitudes less than 0.30.4 ppm could be attributable to TCCON station site-to-site biases (Wunch et al., 2010), so we focus on the biases that are significantly larger and thus most likely attributable to the OCO-2 data. Two clear examples of site-dependent biases are at Edwards, with a mean low bias of ~1.3 ppm, and Wollongong, with a mean high bias of ~0.9 ppm. The spatial dependence of the target-mode measurements reveal that small-scale variability in surface properties (e.g., albedo, altitude, surface roughness) can cause significant and spurious variability in the OCO-2 X_{CO_2}.

The Edwards TCCON station is situated in the bright California high desert on the edge of a very bright playa (with albedos reaching 0.6) with little topographic change . On some, but not all targets (Fig. 6). There have been 12 target observations of Edwards, 10 of which had clear skies during the OCO-2 maneuver. On all but one of the clear-sky target maneuvers over Edwards, the OCO-2 X_{CO_2} appears dependent on surface brightness(Fig. 6). sensitive to surface brightness, with higher X_{CO_2} retrieved over brighter surfaces. However, the magnitude of the sensitivity differs from target to target: the RMS of the target-mode measurements ranges from 0.9 ppm to 1.7 ppm, and the relationship between surface albedo and X_{CO_2} have different slopes (ranging from -2.8 ppm/unit albedo to 10.5 ppm/unit albedo with a mean of 4.5 ppm/unit albedo). The underlying physical reason is currently unknown. All mean target-mode measurements of OCO-2 X_{CO_2} at Edwards are biased lower than the TCCON measurements. coincident TCCON X_{CO_2}.

Conversely, the Wollongong station, which is situated near the East coast of Australia, is a very dark surface in the visible, and lies between the Tasman Sea to the East and the Illawarra Escarpment to the West (Fig. 7). The OCO-2 retrievals of X_{CO_2} in target mode are systematically higher than the TCCON measurements for all target-mode measurementsthose from the TCCON, and are particularly high (up to 5 ppm) in July and August (Fig. 8), due to the problem discussed above in §??below in §4. OCO-2 data over Białystok, located in a dark, forested region, also has a persistent high bias (on the order of 1.31 ppm) compared with TCCON.

Even at sites which do for sites at which OCO-2 X_{CO_2} does not appear to have a significant bias with respect to TCCON, the retrievals can show spurious spatially-correlated errors. The Lauder TCCON station is situated in a valley between rolling hills (Fig. 9). The surface altitude is spatially well-correlated correlated with changes in X_{CO_2} during each target-mode maneuver.

In the standard OCO-2 retrieval algorithm, land surfaces are assumed to have a Lambertian bidirectional reflectance distribution function (BRDF, O'Dell et al., 2012). A more complex BRDF that can better model changes in surface topography and vegetation is currently undergoing testing and shows promise for reducing the problems addressed above (?). An improved treatment of the surface properties will be included in the next version of the OCO-2 dataThe pattern is apparent in all but one clear-sky target-mode measurement over Lauder, and the biases with respect to TCCON are always of the same sign. The RMS of the measurements for each target ranges from 1.0 ppm to 1.9 ppm.

4 Nadir and Glint Mode Comparisons to TCCON

In this section, we evaluate the bias-corrected OCO-2 glint and nadir modes against ground-based TCCON data to reveal mode-dependent other biases that were not eliminated using the standard version 7 bias correction. We use the version 7B B7 retrospective OCO-2 "lite" files here, which have had the footprint-dependent, parameter-dependent, and constant sealing biases removed, and we scaling biases (described in §3) removed. The residual footprint correction was applied manually to the data. The "lite files" are available from the CO_2 Virtual Science Data Environment (JPL-Caltech, 2016, http://co2.jpl.nasa.gov) ar from GES-DISC (2016).

We limit ourselves to data for which the "warn level" is less than or equal to 11~~(Mandrake et al., 2013, 2015), and the "outcome~~, as recommended by Mandrake et al. (2015), and for which the "xco2_quality_flag" is zero. ~~These data are available from the Virtual Science Data Environment (JPL-Caltech, 2016, http://co2.jpl.nasa.gov) and from GES-DISC (2016)~~Mandrake et al. (2015) caution against using warn levels above 12 for nadir and glint modes, because those data can contain errors significantly in excess of the stated a posteriori uncertainties on the X_{CO_2} values. For these comparisons, we choose the following coincidence criteria: a box centred around the TCCON station that spans 5° in latitude and 10° in longitude on the same day as a TCCON measurement, with the exceptions mentioned below. In the southern hemisphere south of 25°S, we use a larger box spanning 20° in latitude and 120° in longitude because the geographical variance in X_{CO_2} in the southern hemisphere is low (e.g., Wunch et al., 2011b). The Edwards and Pasadena boxes are constructed differently because they are geographically very close to each other, but the Pasadena site is within the polluted, mountain-contained South Coast Air Basin, and Edwards is in the clean desert north of the mountains. Thus, we limit the Edwards latitudes to north of Edwards, but allow the longitudes to span 5° further west over the Pacific Ocean. The Pasadena coincidence box is constrained to the South Coast Air Basin, which significantly limits the number of coincident points (see Appendix Figs. A0(a-t)). ~~The median of the measurements~~

The median OCO-2 X_{CO_2} within the coincidence box ~~on the same day as the TCCON measurement~~ recorded on a single day is compared with the TCCON daily median for that day. We choose to compare OCO-2 nadir and glint mode X_{CO_2} with the TCCON daily median values because the median reduces the random component of the TCCON error budget, it is less sensitive to outlier measurements, and it weights the results to local noon where solar zenith angle changes are slowest, and the timing is better matched with the overpass time of OCO-2's orbit. The more complicated dynamical coincidence criteria used to increase the number of coincident measurements between TCCON and GOSAT in Wunch et al. (2011b) and Nguyen et al. (2014) are not required for OCO-2, due to OCO-2's much higher data density.

Figure 10 shows the differences between coincident OCO-2 X_{CO_2} and that from TCCON, separated by viewing mode and season. The bottom panel collects the viewing modes together, still separating by season. The OCO-2 X_{CO_2} appear to have a bias that increases with increasing latitude in the land glint and nadir data north of 45°N (Park Falls). This latitude-dependent bias is consistent with the target-mode results (Fig. 5). A seasonal bias is not apparent at latitudes for which all four seasons have sufficient coincident measurements (Lamont, Edwards, Ascension, Réunion, Wollongong), indicating that the latitudinal bias is not likely caused by an airmass-dependent bias (in either OCO-2 or TCCON). In general, however, the number of coincident measurements is low (Table 3), especially in the northern hemisphere north of 45°N.

In the southern hemisphere winter, there is a significant high bias in the retrieved X_{CO_2} from the OCO-2 ocean glint data. The top panel of figure 10 clearly illustrates this problem by showing the divergence of the OCO-2 X_{CO_2} measurements in ocean glint mode over Wollongong and Lauder from the TCCON X_{CO_2} values during June, July, and August. There were also three target-mode measurements recorded in the southern hemisphere during that time: two points over Wollongong, and a third point over Réunion recorded during late July/early August 2015 that hint at this residual bias (Fig. 4). Appendix Fig. A0 panels (r) and (s) also show this problem as a function of time. This bias does not impact the overall scaling bias between OCO-2 and TCCON X_{CO_2} within the uncertainty but does impact the latitudinal gradients (and hence fluxes) inferred by the OCO-2 data. While the cause of the bias in the southern winter is currently unclear, there is a promising hypothesis related to the OCO-2 algorithm's misrepresentation of stratospheric aerosols, exacerbated by the eruption of Mount Calbuco in Chile on April 22, 2015 (Romero et al., 2016).

The overall comparisons between the OCO-2 data and TCCON data are reported in Tables 3 and 5, and shown in Figs. 11–13 for data from land glint mode, ocean glint mode, and nadir mode. The biases between differences between aggregated, bias-corrected OCO-2 and TCCON are all less than 0.5X_{CO_2} data coincident with all available TCCON daily median measurements are -0.3 ppm, and the RMS of the difference is less than about 1.50.2 ppm., 0.2 ppm for land glint, ocean glint, and nadir, respectively. The RMS values of these differences are 1.3 ppm, 1.4 ppm, and 1.3 ppm, respectively. The differences between the bias-corrected OCO-2 values and the TCCON medians differ from site to site; sites with more than 10 coincident measurements have differences in land glint mode ranging from -0.7 ppm (Wollongong) to 0.9 ppm (Karlsruhe); in ocean glint mode ranging from -1.1 ppm (Saga) to 0.4 ppm (Park Falls); in nadir mode ranging from -0.1 ppm (Wollongong) to 1.6 ppm (Garmisch). Table 4 contains the overall nadir and glint statistics when using warn levels ≤ 15 instead of the recommended warn level filter (≤ 11).

The nadir mode data show the best correlation of the three science modes ($R^2 = 0.75$$R^2 = 0.8$), followed closely by land glint ($R^2 = 0.72$$R^2 = 0.79$), and finally ocean glint ($R^2 = 0.50$$R^2 = 0.66$). The low correlation coefficient in the ocean glint data is partially driven by the high anomalies in the southern hemisphere winter, most obviously in the data over Wollongong (Fig. ??), and also because a high proportion of ocean glint data are in the southern hemisphere, where variability is lower10). If the southern hemisphere winter data (June–September) are excluded from the ocean glint correlations, the R^2 improves to 0.710.76. The slopes of all three curves are significantly different from 1.0. The agreement between the science-mode OCO-2 data and TCCON is poorer than that for the target-mode measurements. Halving the spatial coincidence criteria over each site does not significantly improve the correlation coefficients ($R^2 = 0.78, 0.73, 0.58, 0.77$ for nadir, land glint, ocean glint, and ocean glint excluding the southern hemisphere winter, respectively) and the slopes of the relationship between OCO-2 and TCCON X_{CO_2} increase, but well within the uncertainties. This suggests that it is not solely our definition of the coincidence criteria that causes the low correlation coefficients, and that perhaps the surface properties within the coincidence boxes contain sufficient variability to degrade the comparisons. This highlights the importance of the target-mode data for assessing local, site-to-site, and overall bias.

5 Conclusions

~~The~~ Aggregated OCO-2 X_{CO_2} estimates filtered with warn level ≤ 11 and xco2_quality_flag $= 0$ generally compare well with coincident TCCON data at global scales, with absolute mean biases less than ~~0.5~~0.4 ppm and RMS differences less than ~~about~~ 1.5 ppm. ~~The best comparisons are with the target-mode data, which is expected because the target mode measurement scheme was designed for this purpose. The target-mode data are also particularly well-suited to tying the OCO-2 data to the WMO trace gas scale through comparisons with the TCCON data, because they best represent coincident measurements under invariant atmospheric conditions.~~ While the bias correction clearly improves the relationship between TCCON and OCO-2 globally, ~~smaller-scale biases , typically < 2 , remain. Examples of these biases include spurious~~ some biases remain. Spurious local X_{CO_2} variability that is correlated with topography and surface brightness ~~, and ocean glint measurements at southern~~ is apparent in the target mode measurements, particularly over Edwards, Wollongong and Lauder. Ocean glint measurements from OCO-2 at southern high latitudes during the southern hemisphere winter are biased high, possibly due to stratospheric aerosol interference. In all observation modes, there is an apparent latitude-dependent bias, largest north of 45°N. Remedying these residual biases is the current focus of the OCO-2 algorithm development and validation teams and we anticipate that the next version of the OCO-2 data will represent a significant improvement. It is imperative to continue measurement comparisons with TCCON in all ~~three~~ modes (target, glint and nadir) to monitor and evaluate the OCO-2 data quality throughout its entire mission.

6 Data Availability

Unfiltered, uncorrected OCO-2 data are available from the Goddard Data Center (GES-DISC, 2016). The filtered and bias-corrected data are contained in "lite" files, which are available both from JPL's CO_2 portal ~~(JPL-Caltech, 2016)~~(https://co2.jpl.nasa.gov/, JPL-Caltech, 2016) and the Goddard Data Center. TCCON data are available from the TCCON data archive, hosted by CDIAC: http://tccon.ornl.gov. Each TCCON dataset used in this paper is cited independently in Table 1 or in the captions of Fig. A0.

Appendix A: Site Plots

The ocean glint, land glint and nadir mode plots for each TCCON station are shown in Fig. A0. In each plot, there are four panels. The top left panel shows the time series of the TCCON daily median data (black circles) and the OCO-2 data (triangles coloured differently for each mode). The bottom left panel shows the difference between OCO-2 and TCCON measurements (OCO-2 – TCCON). The top right panel shows the correlations between the TCCON data and the OCO-2 data. The bottom right panel shows the coincidence area for the OCO-2 measurements. Note that the gap in the OCO-2 data over Lauder in winter is caused by near-direct sun glint, during which time the spacecraft is not permitted to measure (i.e., no data were recorded at that latitude during that time).

Appendix B: Author contributions

DW wrote the manuscript and produced the main analysis and results with significant input from GO, CV, and POW. DW, GO, BF, BN, CMR, CO, AE, LM, CV, MRG, DC, and POW contributed to the experiment design and analysis of data. DWTG, NMD, VAV, JN, TW, CP, MdM, MKS, RS, MR, DP, JR, IM, OU, FH, TB, MK, DGF, SGA, KS, JM, RK, PH, LI, JP, PH, SK, MD, HAP, ES, OEGR, YT, PJ, provided TCCON data. All authors read and provided comments on the manuscript.

Acknowledgements. Part of this work was performed at the Jet Propulsion Laboratory, California Institute of Technology, under contract with NASA. Operation of the Ascension Island site was funded by the Max Planck Society. The Bremen, Białystok, and Orléans TCCON sites are funded by the EU projects InGOS and ICOS-INWIRE, and by the Senate of Bremen. The Darwin and Wollongong TCCON sites are funded by NASA grants NAG512247 and NNG05GD07G, and Australian Research Council grants DP140101552, DP110103118, DP0879468, LE0668470, and LP0562346. We are grateful to the DOE ARM program for technical support at the Darwin TCCON site. ND was supported by an Australian Research Council fellowship, DE140100178. The TCCON site at Île de la Réunion is operated by the Royal Belgian Institute for Space Aeronomy with financial support in 2014, 2015 and 2016 under the EU project ICOS-Inwire and the ministerial decree for ICOS (FR/35/IC2) and local activities supported by LACy/UMR8105 - Université de La Réunion. TCCON is funded by NASA grants NNX14AI60G, NNX11AG01G, NAG5-12247, NNG05-GD07G, and NASA's Orbiting Carbon Observatory Program. We are grateful to the DOE ARM program for technical support in Lamont and Jeff Ayers for technical support in Park Falls. From 2004 to 2011 the Lauder TCCON programme was funded by the New Zealand Foundation of Research Science and Technology contracts CO1X0204, CO1X0703 and CO1X0406. Since 2011 the programme has been funded by NIWA's Atmosphere Research Programme 3 (2011/13 Statement of Corporate Intent). The TCCON measurements at Eureka are made by the Canadian Network for the Detection of Atmospheric Change (CANDAC), led by James R. Drummond, and in part by the Canadian Arctic ACE Validation Campaigns, led by Kaley A. Walker. They are supported by the Atlantic Innovation Fund/Nova Scotia Research Innovation Trust, Canada Foundation for Innovation, Canadian Foundation for Climate and Atmospheric Sciences, Canadian Space Agency, Environment Canada, Government of Canada International Polar Year funding, Natural Sciences and Engineering Research Council, Northern Scientific Training Program, Ontario Innovation Trust, Ontario Research Fund and Polar Continental Shelf Program. We thank PEARL site manager Pierre Fogal, the staff at the Eureka weather station, and the CANDAC operators for the logistical and on-site support provided at Eureka. MKD thanks DOE

OBER's TES and NGEE-Tropics program for funding and ARM for logistical support of the TCCON deployment during the GoAmazon campaign.

References

Blumenstock, T., Hase, F., Schneider, M., Garcia, O. E., and Sepulveda, E.: TCCON data from Iza\~{n}a (ES), Release GGG2014R0, TCCON data archive, hosted by CDIAC, doi:10.14291/tccon.ggg2014.izana01.R0/1149295, 2014.

Boland, S., Brown, L. R., Burrows, J. P., Ciais, P., Connor, B. J., Crisp, D., Denning, A. S., Doney, S. C., Engelen, R., Fung, I. Y., Griffith, P., Jacob, D. J., Johnson, B., Martin-Torres, J., Michalak, A. M., Miller, C. E., Polonsky, I., Potter, C., Randerson, J. T., Rayner, P. J., Salawitch, R. J., Santee, M., Tans, P. P., Wennberg, P. O., Wunch, D., Wofsy, S. C., and Yung, Y. L.: The Need for Atmospheric Carbon Dioxide Measurements from Space : Contributions from a Rapid Reflight of the Orbiting Carbon Observatory, Tech. rep., 2009.

Connor, B. J., Boesch, H., Toon, G. C., Sen, B., Miller, C. E., and Crisp, D.: Orbiting Carbon Observatory: Inverse method and prospective error analysis, Journal of Geophysical Research, 113, 1–14, doi:10.1029/2006JD008336, http://www.agu.org/pubs/crossref/2008/2006JD008336.shtml, 2008.

Crisp, D.: Measuring atmospheric carbon dioxide from space with the Orbiting Carbon Observatory-2 (OCO-2), in: SPIE, vol. 9607, pp. 960 702–1, doi:10.1117/12.2187291, http://proceedings.spiedigitallibrary.org/proceeding.aspx?doi=10.1117/12.2187291, 2015.

Crisp, D., Miller, C. E., and DeCola, P. L.: NASA Orbiting Carbon Observatory: measuring the column averaged carbon dioxide mole fraction from space, Journal Of Applied Remote Sensing, 2, 23 508, doi:10.1117/1.2898457, http://scitation.aip.org/getabs/servlet/GetabsServlet?prog=normal{&}id=JARSC4000002000001023508000001{&}idtype=cvips{&}gifs=yes{\T1\textbackslash}npapers2://publication/doi/10.1117/1.2898457, 2008.

Crisp, D., Pollock, H. R., Rosenberg, R., Chapsky, L., Lee, R. A. M., Oyafuso, F. A., Frankenberg, C., O 'dell, C. W., Bruegge, C. J., Doran, G. B., Eldering, A., Fisher, B. M., Fu, D., Gunson, M. R., Mandrake, L., Osterman, G. B., Schwandner, F. M., Sun, K., Taylor, T. E., Wennberg, P. O., and Wunch, D.: The on-orbit performance of the Orbiting Carbon Observatory-2 (OCO-2) instrument and its radiometrically calibrated products, Atmos. Meas. Tech, 10, 59–81, doi:10.5194/amt-10-59-2017, www.atmos-meas-tech.net/10/59/2017/, 2017.

De Mazière, M., Sha, M. K., Desmet, F., Hermans, C., Scolas, F., Kumps, N., Metzger, J.-M., Duflot, V., and Cammas, J.-P.: TCCON data from R\'{e}union Island (RE), Release GGG2014R0, TCCON data archive, hosted by CDIAC, doi:10.14291/tccon.ggg2014.reunion01.R0/1149288, 2014.

Deutscher, N. M., Notholt, J., Messerschmidt, J., Weinzierl, C., Warneke, T., Petri, C., Grupe, P., and Katrynski, K.: TCCON data from Bialystok (PL), Release GGG2014R0, TCCON data archive, hosted by CDIAC, doi:10.14291/tccon.ggg2014.bialystok01.R0/1149277, 2014.

Dubey, M., Henderson, B., Green, D., Butterfield, Z., Keppel-Aleks, G., Allen, N., Blavier, J.-F., Roehl, C., Wunch, D., and Lindenmaier, R.: TCCON data from Manaus (BR), Release GGG2014R0, TCCON data archive, hosted by CDIAC, doi:10.14291/tccon.ggg2014.manaus01.R0/1149274, 2014.

Eldering, A., O'Dell, C. W., Wennberg, P. O., Crisp, D., Gunson, M. R., Viatte, C., Avis, C., Braverman, A., Castano, R., Chang, A., Chapsky, L., Cheng, C., Connor, B., Dang, L., Doran, G., Fisher, B., Frankenberg, C., Fu, D., Granat, R., Hobbs, J., Lee, R. A. M., Mandrake, L., McDuffie, J., Miller, C. E., Myers, V., Natraj, V., O'Brien, D. M., Osterman, G. B., Oyafuso, F., Payne, V. H., Pollock, H. R., Polonsky, I., Roehl, C. M., Rosenberg, R., Schwandner, F., Smyth, M., Tang, V., Taylor, T. E., To, C., Wunch, D., and Yoshimizu, J.: The Orbiting Carbon Observatory-2: First 18 months of Science Data Products, Atmospheric Measurement Techniques Discussions, pp. 1–30, doi:10.5194/amt-2016-247, http://www.atmos-meas-tech-discuss.net/amt-2016-247/, 2016.

Feist, D. G., Arnold, S. G., John, N., and Geibel, M. C.: TCCON data from Ascension Island (SH), Release GGG2014R0, TCCON data archive, hosted by CDIAC, doi:10.14291/tccon.ggg2014.ascension01.R0/1149285, 2014.

Frankenberg, C., O'Dell, C. W., Berry, J., Guanter, L., Joiner, J., Köhler, P., Pollock, R., and Taylor, T. E.: Prospects for chlorophyll fluorescence remote sensing from the Orbiting Carbon Observatory-2, Remote Sensing of Environment, 147, 1–12, doi:10.1016/j.rse.2014.02.007, http://dx.doi.org/10.1016/j.rse.2014.02.007, 2014.

GES-DISC: Goddard Earth Sciences Data and Information Services Center OCO-2 Data Holdings, http://disc.sci.gsfc.nasa.gov/OCO-2, 2016.

Griffith, D. W., Deutscher, N. M., Velazco, V. A., Wennberg, P. O., Yavin, Y., Aleks, G. K., Washenfelder, R. a., Toon, G. C., Blavier, J.-F., Murphy, C., Jones, N., Kettlewell, G., Connor, B. J., Macatangay, R., Roehl, C., Ryczek, M., Glowacki, J., Culgan, T., and Bryant, G.: TCCON data from Darwin (AU), Release GGG2014R0, TCCON data archive, hosted by CDIAC, doi:10.14291/tccon.ggg2014.darwin01.R0/1149290, 2014a.

Griffith, D. W., Velazco, V. A., Deutscher, N. M., Murphy, C., Jones, N., Wilson, S., Macatangay, R., Kettlewell, G., Buchholz, R. R., and Riggenbach, M.: TCCON data from Wollongong (AU), Release GGG2014R0, TCCON data archive, hosted by CDIAC, doi:10.14291/tccon.ggg2014.wollongong01.R0/1149291, 2014b.

Guerlet, S., Butz, A., Schepers, D., Basu, S., Hasekamp, O. P., Kuze, A., Yokota, T., Blavier, J.-F. L., Deutscher, N. M., Griffith, D. W., Hase, F., Kyro, E., Morino, I., Sherlock, V., Sussmann, R., Galli, A., and Aben, I.: Impact of aerosol and thin cirrus on retrieving and validating XCO 2 from GOSAT shortwave infrared measurements, Journal of Geophysical Research: Atmospheres, 118, 4887–4905, doi:10.1002/jgrd.50332, http://doi.wiley.com/10.1002/jgrd.50332, 2013.

Hase, F., Blumenstock, T., Dohe, S., Gross, J., and Kiel, M.: TCCON data from Karlsruhe (DE), Release GGG2014R1, TCCON data archive, hosted by CDIAC, doi:10.14291/tccon.ggg2014.karlsruhe01.R1/1182416, 2014.

Iraci, L. T., Podolske, J., Hillyard, P. W., Roehl, C., Wennberg, P. O., Blavier, J.-F., Allen, N., Wunch, D., Osterman, G., and Albertson, R.: TCCON data from Edwards (US), Release GGG2014R1, TCCON data archive, hosted by CDIAC, doi:10.14291/tccon.ggg2014.edwards01.R1/1255068, 2016.

JPL-Caltech: CO2 Virtual Science Data Environment, http://co2.jpl.nasa.gov, 2016.

Karion, A., Sweeney, C., Tans, P. P., and Newberger, T.: AirCore: An Innovative Atmospheric Sampling System, Journal of Atmospheric and Oceanic Technology, 27, 1839–1853, doi:10.1175/2010JTECHA1448.1, http://journals.ametsoc.org/doi/abs/10.1175/2010JTECHA1448.1, 2010.

Kawakami, S., Ohyama, H., Arai, K., Okumura, H., Taura, C., Fukamachi, T., and Sakashita, M.: TCCON data from Saga (JP), Release GGG2014R0, TCCON data archive, hosted by CDIAC, doi:10.14291/tccon.ggg2014.saga01.R0/1149283, 2014.

Keppel-Aleks, G., Wennberg, P. O., and Schneider, T.: Sources of variations in total column carbon dioxide, Atmospheric Chemistry and Physics, 11, 3581–3593, doi:10.5194/acp-11-3581-2011, http://www.atmos-chem-phys.net/11/3581/2011/, 2011.

Kivi, R., Heikkinen, P., and Kyrö, E.: TCCON data from Sodankyl\"{a} (FI), Release GGG2014R0, TCCON data archive, hosted by CDIAC, doi:10.14291/tccon.ggg2014.sodankyla01.R0/1149280, 2014.

Kuze, A., Suto, H., Nakajima, M., and Hamazaki, T.: Thermal and near infrared sensor for carbon observation Fourier-transform spectrometer on the Greenhouse Gases Observing Satellite for greenhouse gases monitoring., Applied optics, 48, 6716–6733, doi:10.1364/AO.48.006716, http://ao.osa.org/abstract.cfm?URI=ao-48-35-6716{\T1\textbackslash}nhttp://www.opticsinfobase.org/DirectPDFAccess/68E1C66A-0570-929E-8DC1BEA9D7180E52{_}190794/ao-48-35-6716.pdf?da=1{&}id=190794{&}seq=0{&}mobile=no, 2009.

Kuze, A., O'Brien, D. M., Taylor, T. E., Day, J. O., O'Dell, C. W., Kataoka, F., Yoshida, M., Mitomi, Y., Bruegge, C. J., Pollock, H., Basilio, R., Helmlinger, M., Matsunaga, T., Kawakami, S., Shiomi, K., Urabe, T., and Suto, H.: Vicarious Calibration of the GOSAT Sensors Using the Railroad Valley Desert Playa, IEEE Transactions on Geoscience and Remote Sensing, 49, 1781–1795, doi:10.1109/TGRS.2010.2089527, http://ieeexplore.ieee.org/xpls/abs{_}all.jsp?arnumber=5659476http://ieeexplore.ieee.org/lpdocs/epic03/wrapper.htm?arnumber=5659476, 2011.

Kuze, A., Suto, H., Shiomi, K., Kawakami, S., Tanaka, M., Ueda, Y., Deguchi, A., Yoshida, J., Yamamoto, Y., Kataoka, F., Taylor, T. E., and Buijs, H.: Update on GOSAT TANSO-FTS performance, operations, and data products after more than six years in space, Atmospheric Measurement Techniques Discussions, 2014, 1–38, doi:10.5194/amt-2015-333, http://www.atmos-meas-tech-discuss.net/amt-2015-333/, 2016.

Mandrake, L., Frankenberg, C., O'Dell, C. W., Osterman, G., Wennberg, P. O., and Wunch, D.: Semi-autonomous sounding selection for OCO-2, Atmospheric Measurement Techniques, 6, 2851–2864, doi:10.5194/amt-6-2851-2013, http://www.atmos-meas-tech.net/6/2851/2013/, 2013.

Mandrake, L., O'Dell, C. W., Wunch, D., Wennberg, P. O., Fisher, B., Osterman, G. B., and Eldering, A.: Orbiting Carbon Observatory-2 (OCO-2) Warn Level, Bias Correction, and Lite File Product Description, Tech. rep., Jet Propulsion Laboratory, California Institute of Technology, Pasasdena, http://disc.sci.gsfc.nasa.gov/OCO-2/documentation/oco-2-v7/OCO2{_}XCO2{_}Lite{_}Files{_}and{_}Bias{_}Correction{_}0915{_}sm.pdf, 2015.

McGill, R., Tukey, J. W., and Larsen, W. a.: Variations of Box Plots, The American Statistician, 32, 12–16, doi:10.2307/2683468, 1978.

Messerschmidt, J., Geibel, M. C., Blumenstock, T., Chen, H., Deutscher, N. M., Engel, A., Feist, D. G., Gerbig, C., Gisi, M., Hase, F., Katrynski, K., Kolle, O., Lavrič, J. V., Notholt, J., Palm, M., Ramonet, M., Rettinger, M., Schmidt, M., Sussmann, R., Toon, G. C., Truong, F., Warneke, T., Wennberg, P. O., Wunch, D., and Xueref-Remy, I.: Calibration of TCCON column-averaged CO2: the first aircraft campaign over European TCCON sites, Atmospheric Chemistry and Physics, 11, 10 765–10 777, doi:10.5194/acp-11-10765-2011, http://www.atmos-chem-phys.net/11/10765/2011/, 2011.

Morino, I., Matsuzaki, T., and Shishime, A.: TCCON data from Tsukuba (JP), 125HR, Release GGG2014R1, TCCON data archive, hosted by CDIAC, doi:10.14291/tccon.ggg2014.tsukuba02.R1/1241486, 2014a.

Morino, I., Yokozeki, N., Matzuzaki, T., and Horikawa, M.: TCCON data from Rikubetsu (JP), Release GGG2014R1, TCCON data archive, hosted by CDIAC, doi:10.14291/tccon.ggg2014.rikubetsu01.R1/1242265, 2014b.

Nguyen, H., Osterman, G., Wunch, D., O'Dell, C. W., Mandrake, L., Wennberg, P. O., Fisher, B., and Castano, R.: A method for colocating satellite XCO2 data to ground-based data and its application to ACOS-GOSAT and TCCON, Atmospheric Measurement Techniques, 7, 2631–2644, doi:10.5194/amt-7-2631-2014, http://www.atmos-meas-tech.net/7/2631/2014/, 2014.

Notholt, J., Petri, C., Warneke, T., Deutscher, N. M., Buschmann, M., Weinzierl, C., Macatangay, R., and Grupe, P.: TCCON data from Bremen (DE), Release GGG2014R0, TCCON data archive, hosted by CDIAC, doi:10.14291/tccon.ggg2014.bremen01.R0/1149275, 2014.

O'Dell, C. W., Connor, B. J., Bösch, H., O'Brien, D. M., Frankenberg, C., Castano, R., Christi, M., Eldering, D., Fisher, B., Gunson, M., McDuffie, J., Miller, C. E., Natraj, V., Oyafuso, F. A., Polonsky, I., Smyth, M., Taylor, T. E., Toon, G. C., Wennberg, P. O., and Wunch, D.: The ACOS CO2 retrieval algorithm – Part 1: Description and validation against synthetic observations, Atmospheric Measurement Techniques, 5, 99–121, doi:10.5194/amt-5-99-2012, http://www.atmos-meas-tech.net/5/99/2012/, 2012.

Pan, L. L., Bowman, K. P., Atlas, E. L., Wofsy, S. C., Zhang, F., Bresch, J. F., Ridley, B. A., Pittman, J. V., Homeyer, C. R., Romashkin, P. A., and Cooper, W. A.: The Stratosphere–Troposphere Analyses of Regional Transport 2008 Experiment, Bulletin of the American Meteorological Society, 91, 327–342, doi:10.1175/2009BAMS2865.1, http://journals.ametsoc.org/doi/abs/10.1175/2009BAMS2865.1, 2010.

Romero, J. E., Morgavi, D., Arzilli, F., Daga, R., Caselli, A., Reckziegel, F., Viramonte, J., Díaz-Alvarado, J., Polacci, M., Burton, M., and Perugini, D.: Eruption dynamics of the 22-23 April 2015 Calbuco Volcano (Southern Chile): Analyses of tephra fall deposits, Journal of Volcanology and Geothermal Research, 317, 15–29, doi:10.1016/j.jvolgeores.2016.02.027, http://dx.doi.org/10.1016/j.jvolgeores.2016.02.027, 2016.

Schneising, O., Bergamaschi, P., Bovensmann, H., Buchwitz, M., Burrows, J. P., Deutscher, N. M., Griffith, D. W., Heymann, J., Macatangay, R., Messerschmidt, J., Notholt, J., Rettinger, M., Reuter, M., Sussmann, R., Velazco, V. A., Warneke, T., Wennberg, P. O., and Wunch, D.: Atmospheric greenhouse gases retrieved from SCIAMACHY: comparison to ground-based FTS measurements and model results, Atmospheric Chemistry and Physics, 12, 1527–1540, doi:10.5194/acp-12-1527-2012, http://www.atmos-chem-phys.net/12/1527/2012/, 2012.

Sherlock, V., Connor, B. J., Robinson, J., Shiona, H., Smale, D., and Pollard, D.: TCCON data from Lauder (NZ), 125HR, Release GGG2014R0, TCCON data archive, hosted by CDIAC, doi:10.14291/tccon.ggg2014.lauder02.R0/1149298, 2014.

Singh, H. B., Brune, W. H., Crawford, J. H., Jacob, D. J., and Russell, P. B.: Overview of the summer 2004 Intercontinental Chemical Transport Experiment-North America (INTEX-A), Journal of Geophysical Research: Atmospheres, 111, doi:10.1029/2006JD007905, 2006.

Strong, K., Mendonca, J., Weaver, D., Fogal, P., Drummond, J., Batchelor, R., and Lindenmaier, R.: TCCON data from Eureka (CA), Release GGG2014R0, TCCON data archive, hosted by CDIAC, doi:10.14291/tccon.ggg2014.eureka01.R0/1149271, 2014.

Sussmann, R. and Rettinger, M.: TCCON data from Garmisch (DE), Release GGG2014R0, TCCON data archive, hosted by CDIAC, doi:10.14291/tccon.ggg2014.garmisch01.R0/1149299, 2014.

Te, Y., Jeseck, P., and Janssen, C.: TCCON data from Paris (FR), Release GGG2014R0, TCCON data archive, hosted by CDIAC, doi:10.14291/tccon.ggg2014.paris01.R0/1149279, 2014.

Warneke, T., Messerschmidt, J., Notholt, J., Weinzierl, C., Deutscher, N. M., Petri, C., Grupe, P., Vuillemin, C., Truong, F., Schmidt, M., Ramonet, M., and Parmentier, E.: TCCON data from Orl\'{e}ans (FR), Release GGG2014R0, TCCON data archive, hosted by CDIAC, doi:10.14291/tccon.ggg2014.orleans01.R0/1149276, 2014.

Washenfelder, R. A., Toon, G. C., Blavier, J.-F. L., Yang, Z., Allen, N. T., Wennberg, P. O., Vay, S. A., Matross, D. M., and Daube, B. C.: Carbon dioxide column abundances at the Wisconsin Tall Tower site, Journal of Geophysical Research, 111, 1–11, doi:10.1029/2006JD007154, http://www.agu.org/pubs/crossref/2006/2006JD007154.shtml, 2006.

Wennberg, P. O., Roehl, C., Wunch, D., Toon, G. C., Blavier, J.-F., Washenfelder, R. a., Keppel-Aleks, G., Allen, N., and Ayers, J.: TCCON data from Park Falls (US), Release GGG2014R0, TCCON data archive, hosted by CDIAC, doi:10.14291/tccon.ggg2014.parkfalls01.R0/1149161, 2014a.

Wennberg, P. O., Wunch, D., Roehl, C., Blavier, J.-F., Toon, G. C., and Allen, N.: TCCON data from Caltech (US), Release GGG2014R1, TCCON data archive, hosted by CDIAC, doi:10.14291/tccon.ggg2014.pasadena01.R1/1182415, 2014b.

Wennberg, P. O., Wunch, D., Roehl, C., Blavier, J.-F. L., Toon, G. C., and Allen, N.: TCCON data from California Institute of Technology, Pasadena, California, USA, Release GGG2014R1, TCCON data archive, hosted by the Carbon Dioxide Information Analysis Center, Oak Ridge National Laboratory, Oak Ridge, Tennessee, U.S.A., http://dx.doi.org/10.14291/tccon.ggg2014.pasadena01.R1/1182415, doi:10.14291/tccon.ggg2014.pasadena01.R1/1182415, 2014c.

Wennberg, P. O., Wunch, D., Roehl, C., Blavier, J.-F., Toon, G. C., Allen, N., Dowell, P., Teske, K., Martin, C., and Martin., J.: TCCON data from Lamont (US), Release GGG2014R1, TCCON data archive, hosted by CDIAC, doi:10.14291/tccon.ggg2014.lamont01.R1/1255070, 2016.

Wofsy, S. C.: HIAPER Pole-to-Pole Observations (HIPPO): fine-grained, global-scale measurements of climatically important atmospheric gases and aerosols., Philosophical Transactions of the Royal Society - Series A: Mathematical, Physical and Engineering Sciences, 369, 2073–86, doi:10.1098/rsta.2010.0313, http://www.ncbi.nlm.nih.gov/pubmed/21502177, 2011.

Wunch, D., Toon, G. C., Wennberg, P. O., Wofsy, S. C., Stephens, B. B., Fischer, M. L., Uchino, O., Abshire, J. B., Bernath, P. F., Biraud, S. C., Blavier, J.-F. L., Boone, C., Bowman, K. P., Browell, E. V., Campos, T., Connor, B. J., Daube, B. C., Deutscher, N. M., Diao, M., Elkins, J. W., Gerbig, C., Gottlieb, E., Griffith, D. W., Hurst, D. F., Jiménez, R., Keppel-Aleks, G., Kort, E. A., MacAtangay, R., MacHida, T., Matsueda, H., Moore, F., Morino, I., Park, S., Robinson, J., Roehl, C. M., Sawa, Y., Sherlock, V., Sweeney, C., Tanaka, T., and Zondlo, M. a.: Calibration of the total carbon column observing network using aircraft profile data, Atmospheric Measurement Techniques, 3, 1351–1362, doi:10.5194/amt-3-1351-2010, http://www.atmos-meas-tech.net/3/1351/2010/, 2010.

Wunch, D., Toon, G. C., Blavier, J.-F. L., Washenfelder, R. A., Notholt, J., Connor, B. J., Griffith, D. W., Sherlock, V., and Wennberg, P. O.: The total carbon column observing network., Philosophical transactions. Series A, Mathematical, physical, and engineering sciences, 369, 2087–

2112, doi:10.1098/rsta.2010.0240, http://rsta.royalsocietypublishing.org/content/369/1943/2087http://www.ncbi.nlm.nih.gov/pubmed/21502178, 2011a.

Wunch, D., Wennberg, P. O., Toon, G. C., Connor, B. J., Fisher, B., Osterman, G. B., Frankenberg, C., Mandrake, L., O'Dell, C. W., Ahonen, P., Biraud, S. C., Castano, R., Cressie, N., Crisp, D., Deutscher, N. M., Eldering, A., Fisher, M. L., Griffith, D. W., Gunson, M., Heikkinen, P., Keppel-Aleks, G., Kyrö, E., Lindenmaier, R., MacAtangay, R., Mendonca, J., Messerschmidt, J., Miller, C. E., Morino, I., Notholt, J., Oyafuso, F. A., Rettinger, M., Robinson, J., Roehl, C. M., Salawitch, R. J., Sherlock, V., Strong, K., Sussmann, R., Tanaka, T., Thompson, D. R., Uchino, O., Warneke, T., and Wofsy, S. C.: A method for evaluating bias in global measurements of CO2 total columns from space, Atmospheric Chemistry and Physics, 11, 12 317–12 337, doi:10.5194/acp-11-12317-2011, http://www.atmos-chem-phys.net/11/12317/2011/, 2011b.

Wunch, D., Toon, G. C., Sherlock, V., Deutscher, N. M., Liu, C., Feist, D. G., and Wennberg, P. O.: The Total Carbon Column Observing Network's GGG2014 Data Version, Tech. rep., California Institute of Technology, Carbon Dioxide Information Analysis Center, Oak Ridge National Laboratory, Oak Ridge, Tennessee, U.S.A., doi:10.14291/tccon.ggg2014.documentation.R0/1221662, http://dx.doi.org/10.14291/tccon.ggg2014.documentation.R0/1221662, 2015.

Yang, Z., Washenfelder, R. a., Keppel-Aleks, G., Krakauer, N. Y., Randerson, J. T., Tans, P. P., Sweeney, C., and Wennberg, P. O.: New constraints on Northern Hemisphere growing season net flux, Geophysical Research Letters, 34, L12 807, doi:10.1029/2007GL029742, http://www.agu.org/pubs/crossref/2007/2007GL029742.shtml, 2007.

York, D., Evensen, N. M., Martinez, M. L., and De Basabe Delgado, J.: Unified equations for the slope, intercept, and standard errors of the best straight line, American Journal of Physics, 72, 367, doi:10.1119/1.1632486, http://link.aip.org/link/AJPIAS/v72/i3/p367/s1{&}Agg=doi, 2004.

Zhao, C. L. and Tans, P. P.: Estimating uncertainty of the WMO mole fraction scale for carbon dioxide in air, Journal of Geophysical Research, 111, 1–10, doi:10.1029/2005JD006003, http://www.agu.org/pubs/crossref/2006/2005JD006003.shtml, 2006.

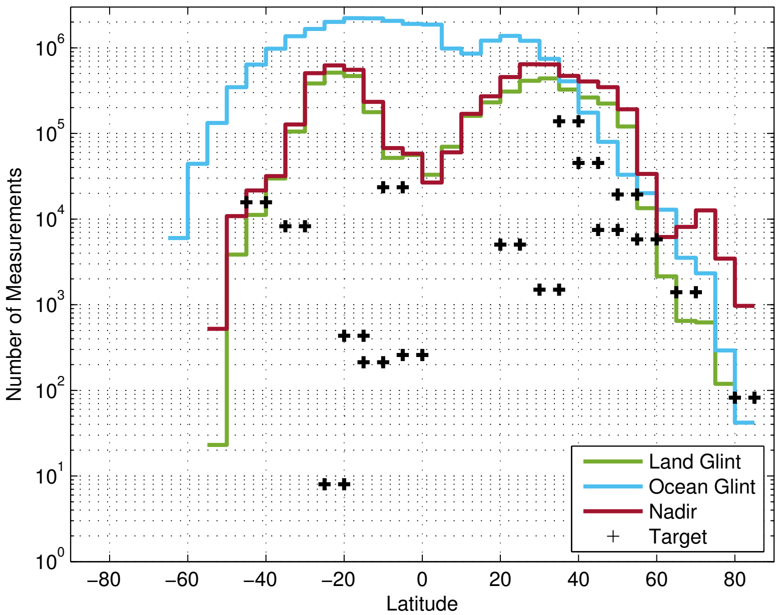

Figure 1: ~~Nadir~~OCO-2 nadir, ~~and~~ glint, and target-mode measurement density in 5° bins as a function of latitude from the beginning of the mission through ~~April 30~~December 31, 2016. These are from the "lite" files applying "warn level" 11 filters and requiring that the "~~outcome~~xco2_quality_flag" is zero.

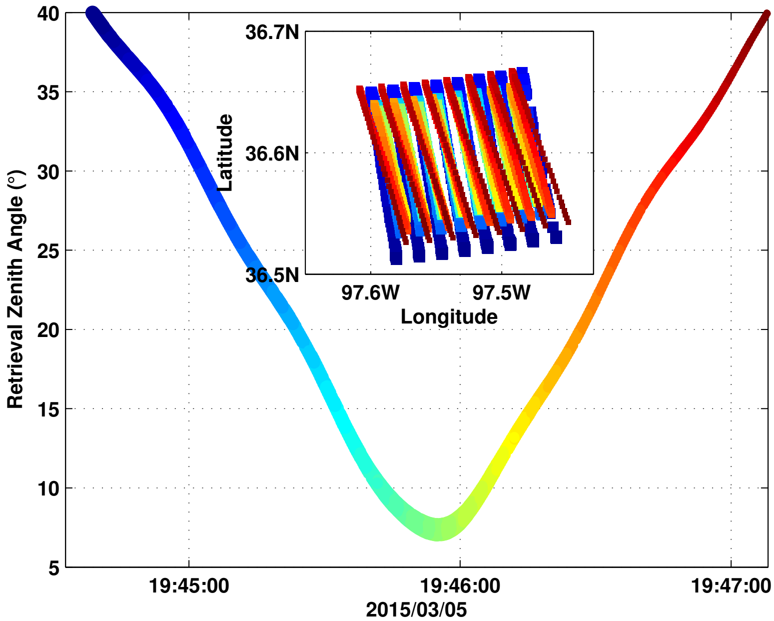

Figure 2: The zenith angles viewed during ~~a~~ an OCO-2 target mode ~~measurement~~ maneuver over Lamont ~~.~~ on March 5, 2015. The spacecraft “nods" across the ground target as it rotates overhead. The colours ~~represent~~ and decreasing size of the points indicate the time of the measurement. The top inset shows the locations of the measurements in latitude and longitude. The 8 footprints are apparent in the roughly N-S stripes. There are 3,473 soundings with a retrieval zenith angle of less than 40 degrees in this target-mode maneuver, most of which are obscured in the inset by the later, nearly spatially coincident soundings.

Figure 3: Map of OCO-2 target locations. ~~Gold~~ Yellow circles show the locations of the targets that coincide with TCCON stations; orange stars show the locations of targets that do not have co-located TCCON stations.

The number of target mode maneuvers attempted per month (left axis), and the cumulative number of target mode maneuvers attempted to date (right axis). The TCCON targets are in grey squares; all targets (including Railroad Valley, which does not have a TCCON station) are marked in black circles.

~~The relationship between the OCO-2 target-mode data and the coincident TCCON data. The top plot (a) does not have the Mandrake et al. (2015) bias correction applied, the bottom plot (b) is after bias correction, but before the scaling is applied. The one-to-one line is indicated by the dashed black line, and the best fit is marked in the solid black~~

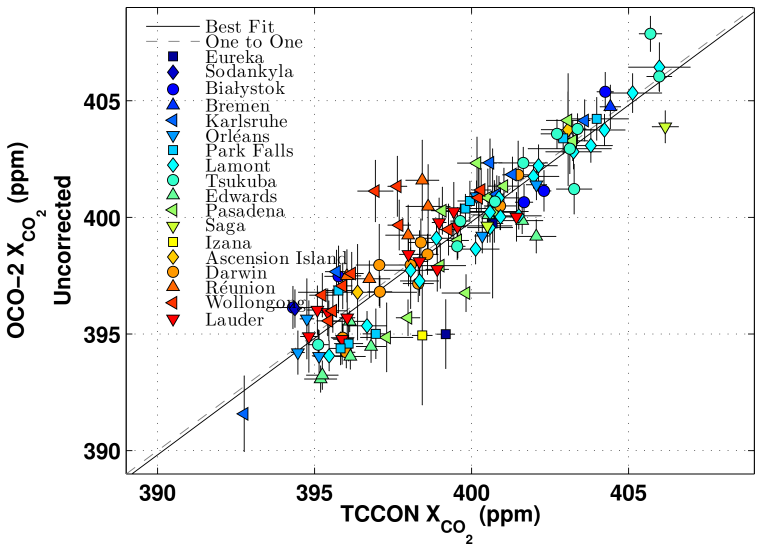

~~line.~~

(a) Without bias correction.

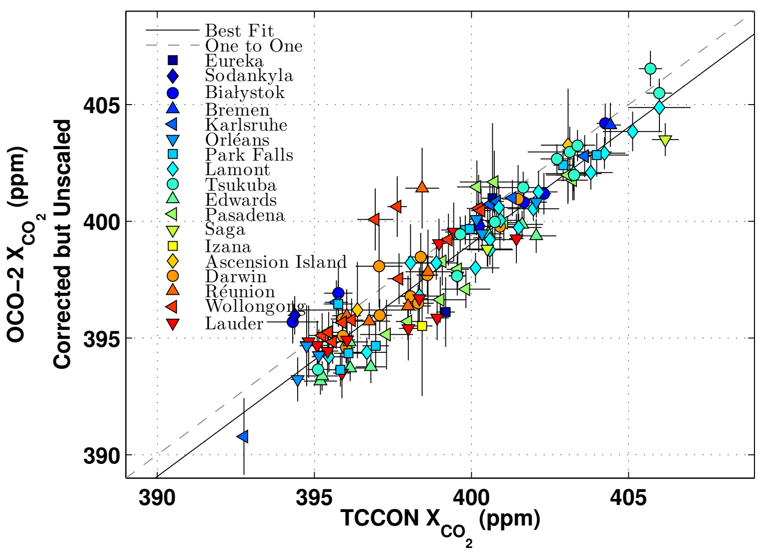

(b) With bias correction but without scaling.

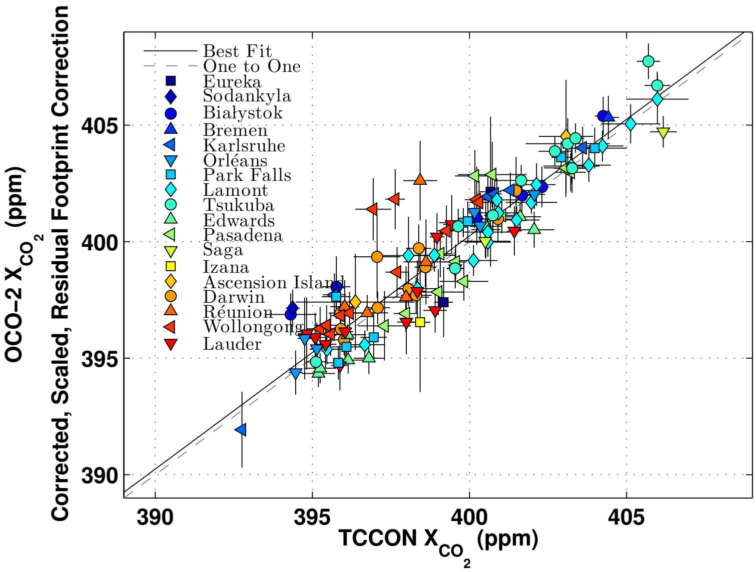

(c) With bias correction, scaling correction, and residual footprint dependent correction.

Figure 3: The relationship between the median value from each OCO-2 target-mode maneuver and the median value of the coincident TCCON data, typically recorded with one hour of the maneuver. The top plot (a) does not have the Mandrake et al. (2015) bias correction applied, the middle plot (b) is after bias correction, but before the scaling is applied. Plot (c) shows the relationship when the scaling correction is applied, as well as the recommended residual footprint correction described in Mandrake et al. (2015). The slope and scatter in plot (c) is unaffected by the residual footprint correction. The one-to-one line is indicated by the dashed line, and the best fit is marked in the solid line. The error bars represent the standard deviation about the median.

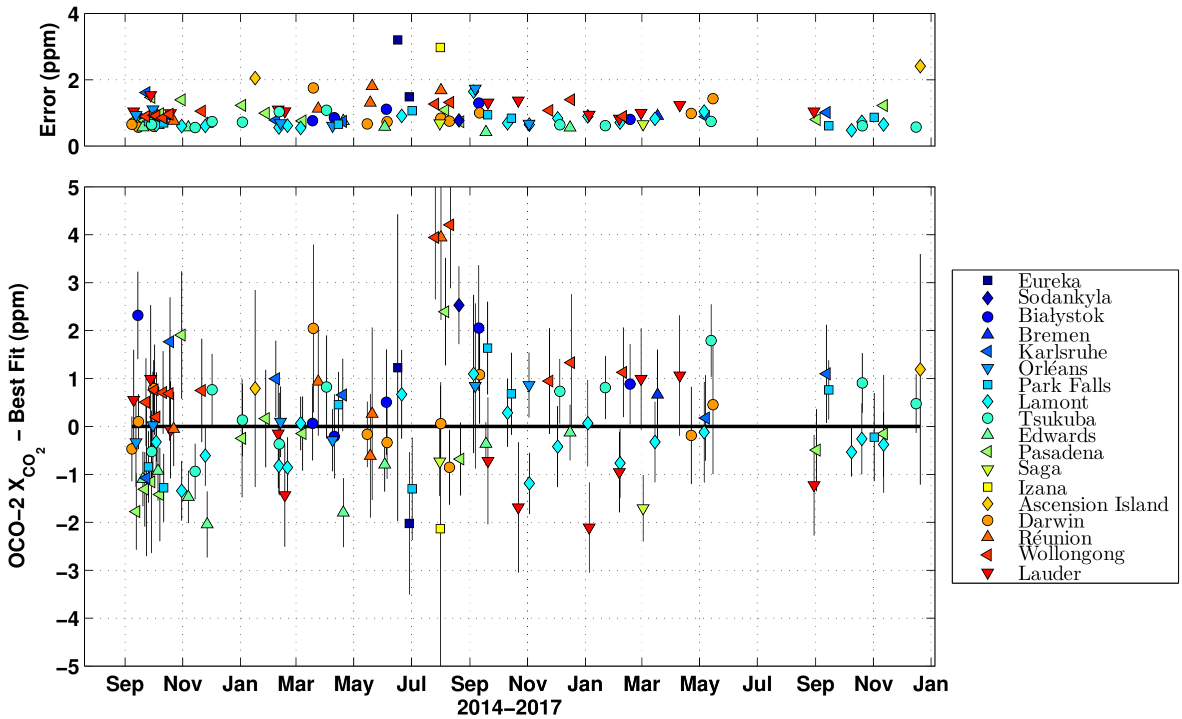

Figure 4: The time series of the differences between the OCO-2 target-mode data and the best fit line in Fig. 3(~~b~~c). The top panel shows the magnitude of the sum in quadrature of the standard deviation of the OCO-2 data during the target and the standard deviation of the coincident TCCON data. Those values are plotted as the error bars in the lower panel.

~~The latitudinal gradient of OCO-2 data in August 2015 (left), and in October 2015 (right). The grey squares are monthly mean OCO-2 data from glint and nadir mode gridded in $0.5°\times0.5°$ bins. The black circles are the OCO-2 zonal means after gridding onto a $4°\times5°$ grid. The error bars indicate the 1σ standard deviation. The TCCON monthly medians are marked by the squares with 1σ standard deviation error bars. The colours represent the fossil fuel emissions within 50 of the TCCON location. The fossil fuel emission source is from the European Commission, Joint Research Centre (JRC)/Netherlands Environmental Assessment Agency (PBL). Emission Database for Global Atmospheric Research (EDGAR), http://edgar.jrc.ec.europe.eu. The high bias of the OCO-2 data in the higher latitude southern hemisphere (which is dominated by glint measurements over water) is clearly evident in the August plot south of -20°.~~

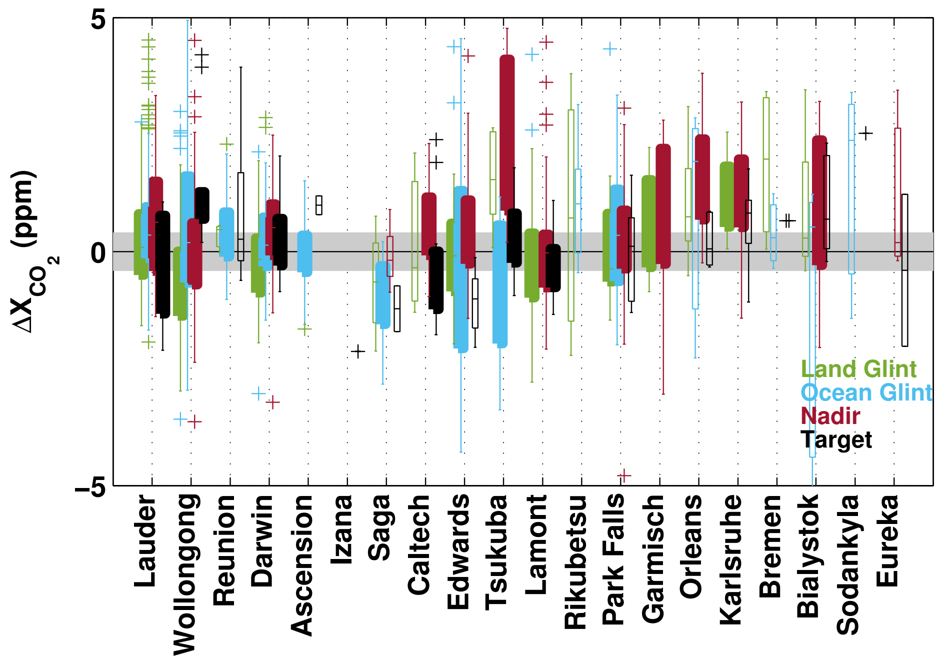

Figure 5: The site-to-site differences between the OCO-2 ~~target-mode~~ data and the coincident TCCON data, separated by observation mode. This is a "box plot": the ~~circles indicate the median value~~ bottom and top edges of the ~~difference, the thick bars~~ box indicate the 25 and 75 percentile limits, ~~the thin bars~~ whiskers represent the full range of the data, excluding the outliers (McGill et al., 1978). The outliers and sites for which only one coincident set of measurements are available are represented by plus ('+') symbols. The grey shaded area indicates the ~~±0.3~~±0.4 ppm uncertainty in the TCCON values: deviations beyond the shading ~~can be attributed~~ are more likely attributable to uncertainties in the OCO-2 data. Filled boxes indicate sites for which more than 10 coincident measurements were made. Open boxes have at least three coincident measurements.

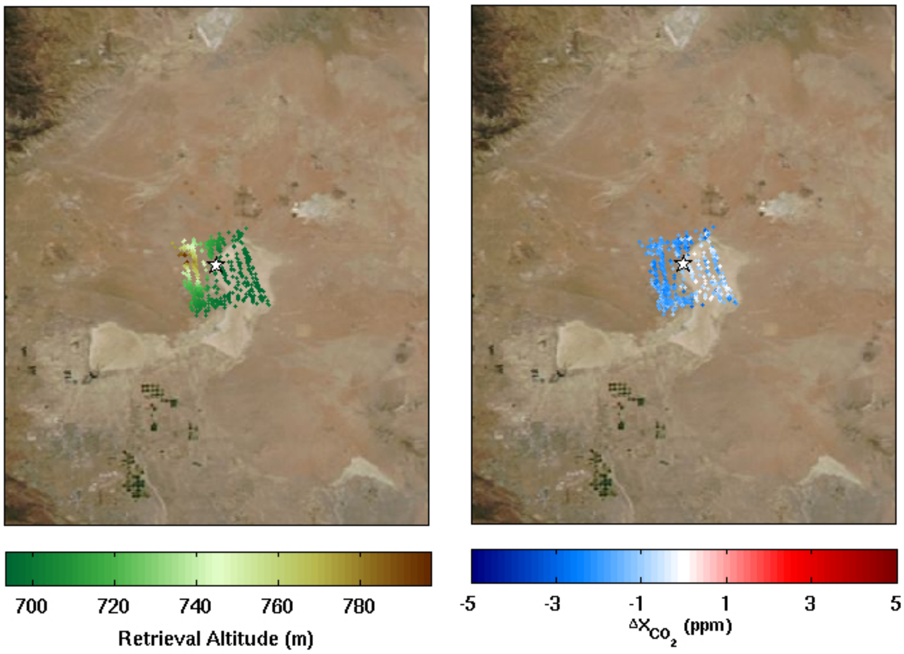

Figure 6: Edwards target on April 19, 2015. The background is the MODIS true-colour image of the Edwards area at the time of the target-mode ~~measurements~~maneuvers. The white star indicates the location of the Edwards TCCON station. The left panel shows the elevation model of the surface and the right panel shows the difference in OCO-2 X_{CO_2} from the value recorded by the TCCON instrument. A spatial bias related to the surface brightness is clearly present in this target-mode measurement. In other Edwards target mode measurements, this surface brightness-correlated bias is not as ~~apparent~~strong.

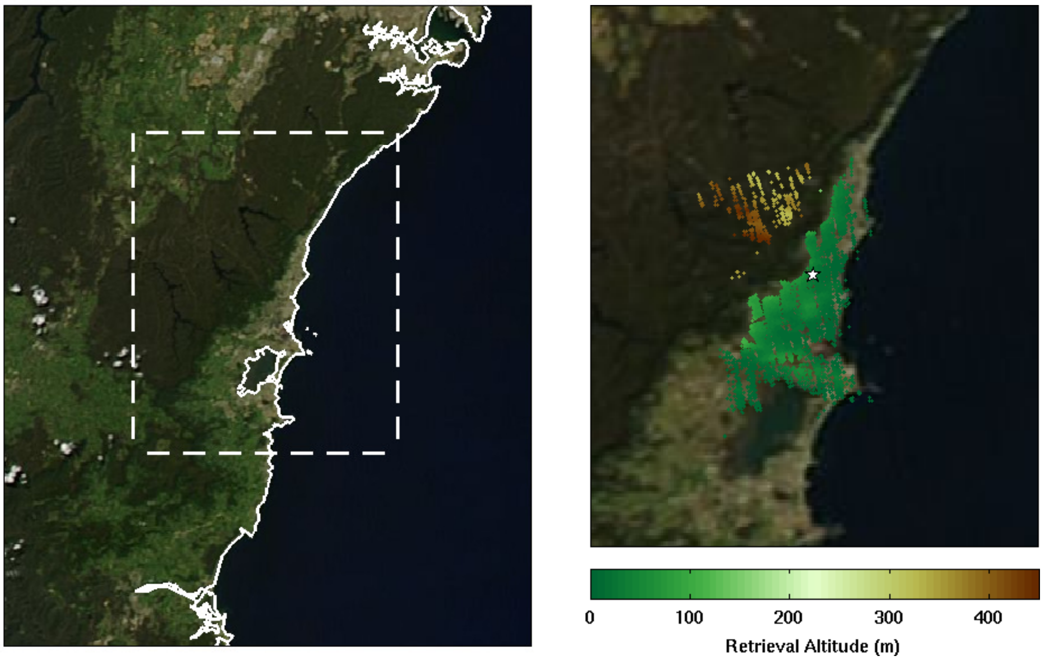

(a) (b)

Figure 7: ~~The retrieval altitudes near~~ Panel (a) above shows the MODIS true-colour image of the Wollongong ~~TCCON station during target measurements~~region. The white solid line marks the east coast of Australia; the South Pacific (Tasman Sea) lies to the east. The sharp Illawarra escarpment ~~can be clearly seen~~ is the dark region inland~~from~~ , mostly contained in the ~~Tasman Sea (to~~ dashed white box. The dashed white box shows the ~~East~~latitude and longitude extent of the images in panel (b) and in Fig. 8. Panel (b) shows the retrieval altitudes near the Wollongong TCCON station compiled from several target maneuvers.

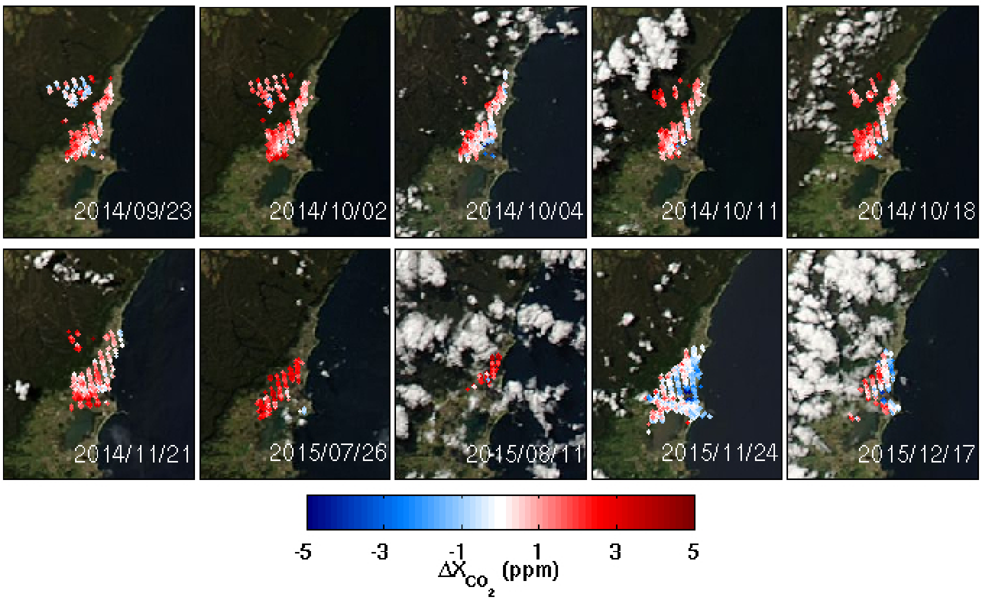

Figure 8: The filtered target-mode measurements over Wollongong. The colours represent the difference between the OCO-2 measurement and the coincident TCCON measurement. The OCO-2 data over Wollongong are generally higher (redder) than the TCCON measurements, and significantly high in the July and August 2015 target-mode maneuvers.

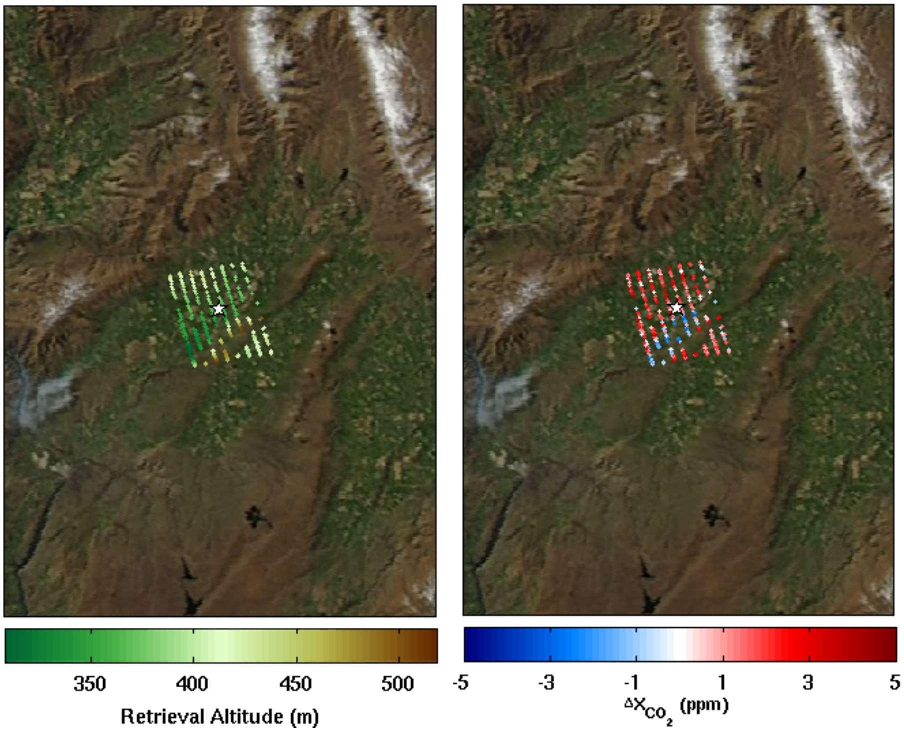

Figure 9: Lauder target on September 28, 2014. The background is the MODIS true-colour image of the Lauder area at the time of the target-mode ~~measurements~~maneuvers. The white star indicates the location of the Lauder TCCON station. The left panel shows the elevation model of the surface and the right panel shows the difference in X_{CO_2} from the value recorded by the TCCON instrument. A spatial bias is clearly present, related to the surface elevation.

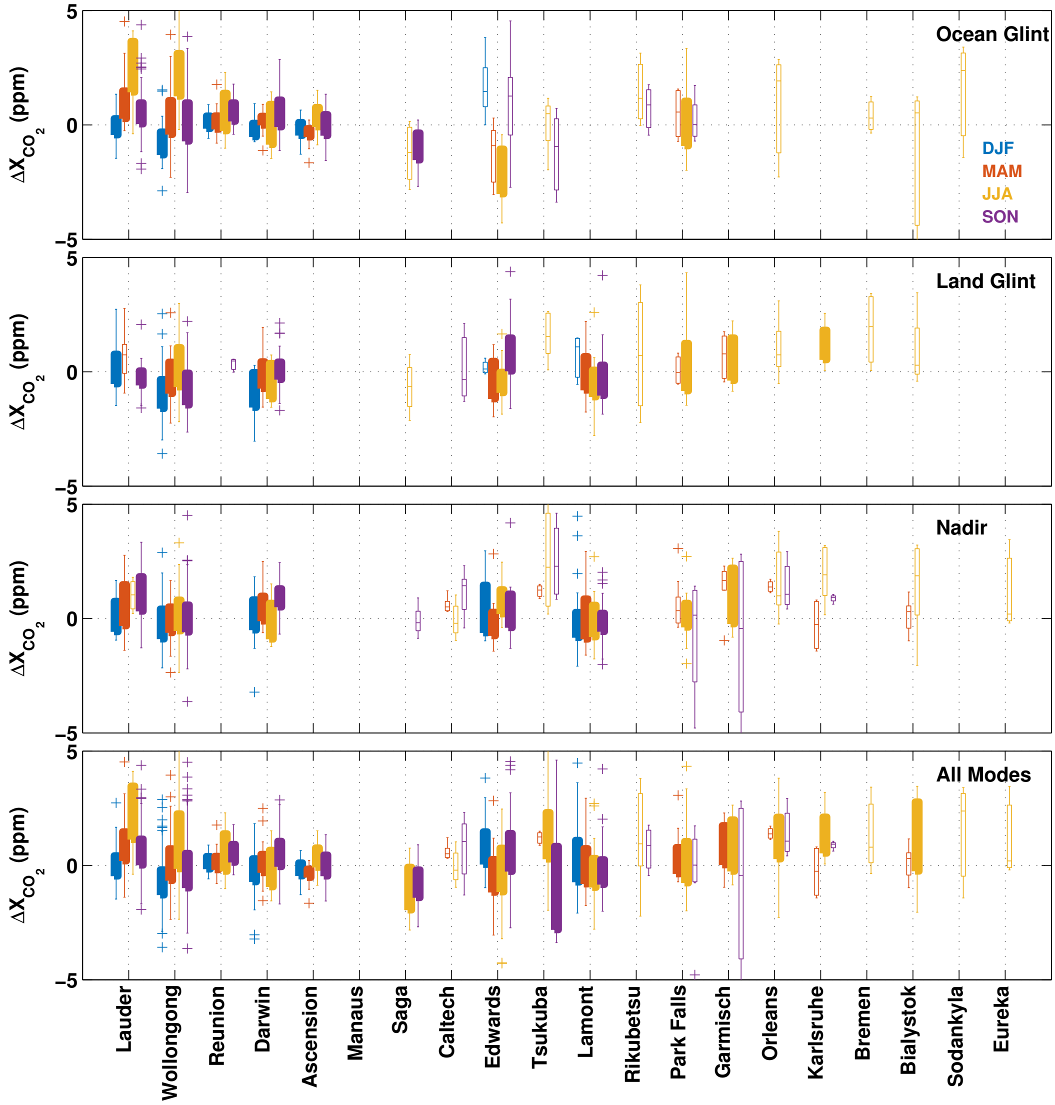

Figure 10: The dependence of the difference between OCO-2 X_{CO_2} coincident with TCCON X_{CO_2} (ΔX_{CO_2}) on the season and OCO-2 observing mode. The filled boxes indicate seasons for which there are >10 comparison points between OCO-2 and TCCON; the thin boxes contain at least 3 comparison points. Any site and season for which there were fewer than three comparison points were excluded from the plot. The different colours indicate the different seasons (blue = DJF, orange = MAM, yellow = JJA, purple = SON). The TCCON stations are ordered by latitude, where Lauder is 45°S and Eureka is 80°N. The equator is between Manaus (3°S) and Saga (33°N). The high southern latitude ocean glint bias is clear in the top plot.

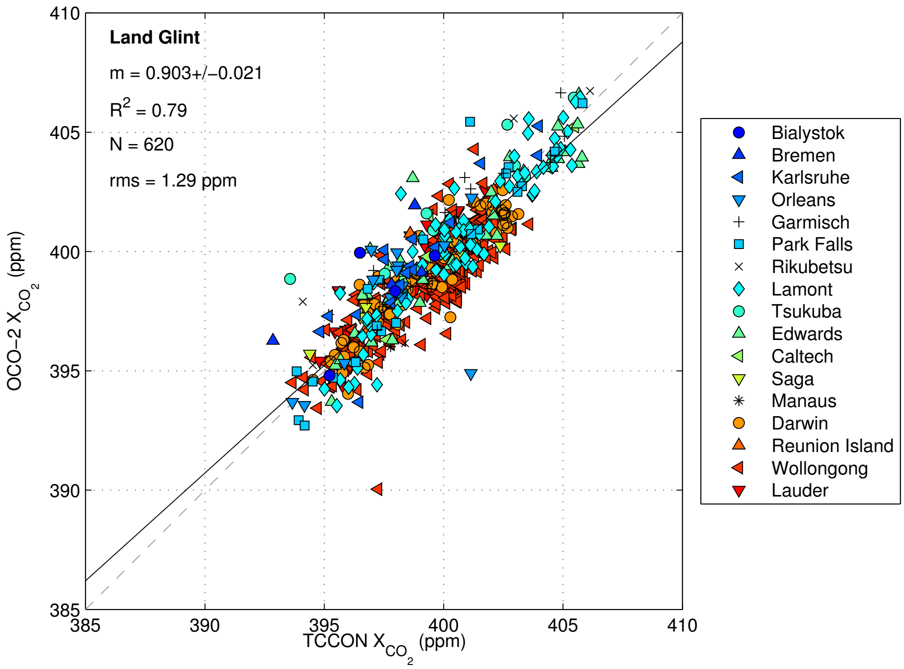

Figure 11: Land glint OCO-2 one-to-one plot against TCCON. The slope of the relationship is represented by "m" in the figure, and the coefficient of determination is represented by "R^2". The number of points on the graph is indicated by "N" and the root-mean-square value (rms) of the differences between OCO-2 and TCCON X_{CO_2} is also shown. Many points are overlaid in this graph, obscuring the density of points along the best fit line.

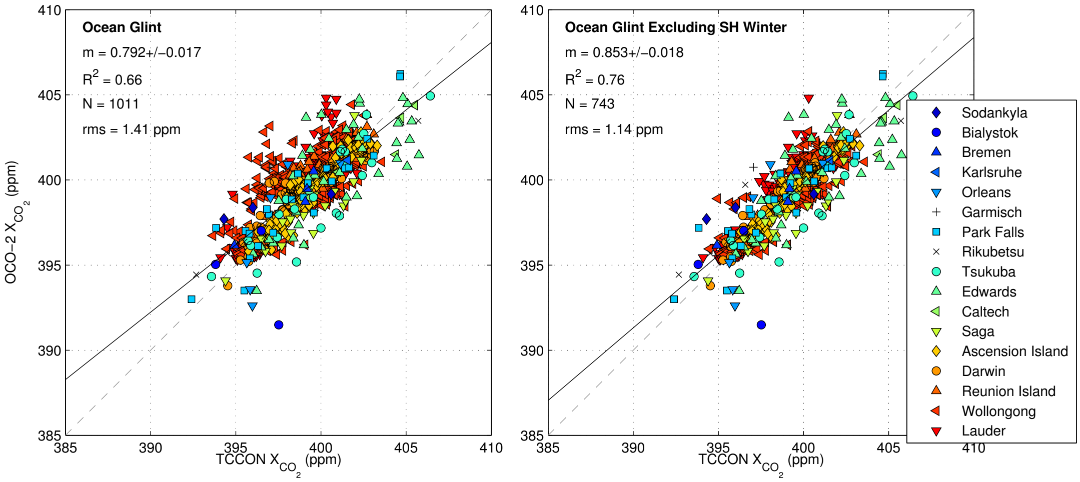

Figure 12: Ocean glint OCO-2 one-to-one plot against TCCON. The left panel shows all the glint-mode data. The right panel removes the southern hemisphere wintertime (June through September) glint data that has a known high bias. The annotations follow those in Fig. 11.

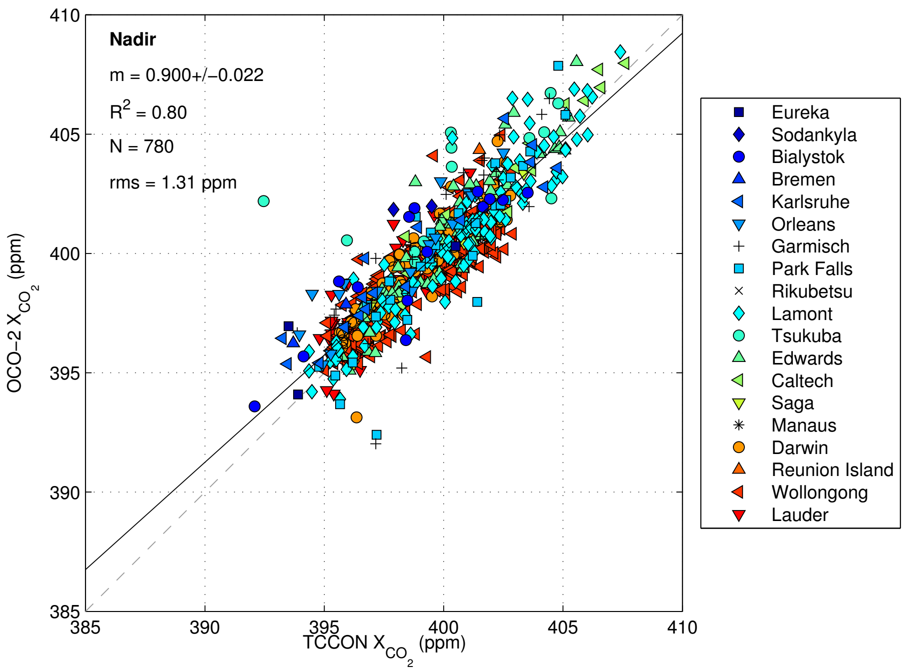

Figure 13: Nadir OCO-2 one-to-one plot against TCCON. The annotations follow those in Fig. 11.

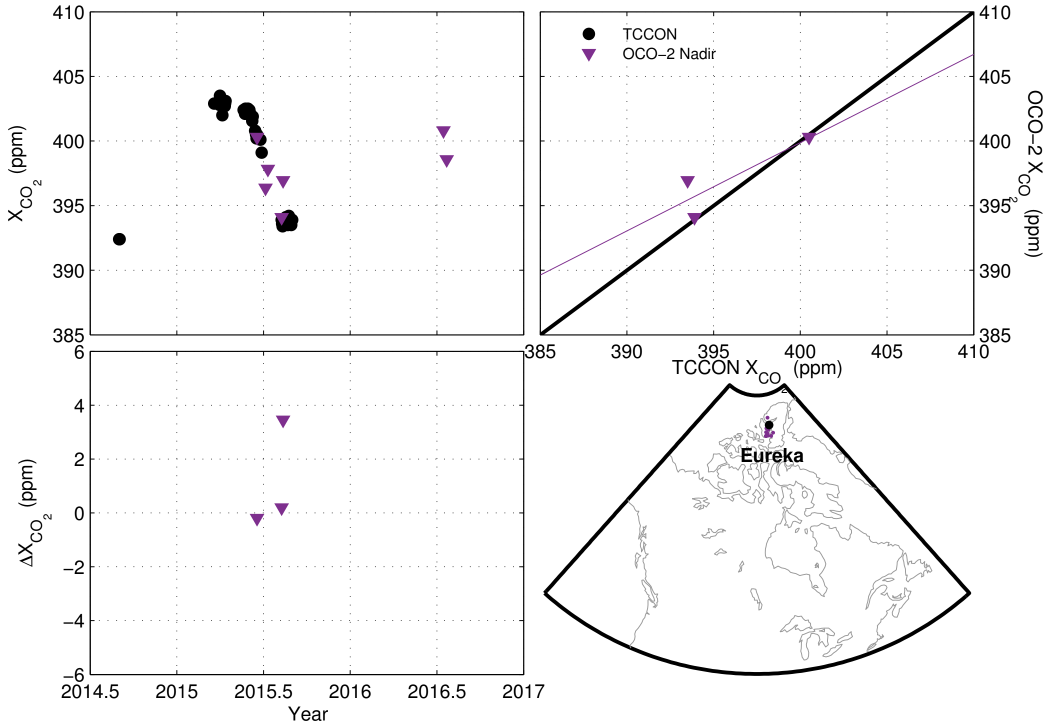

(a) Eureka

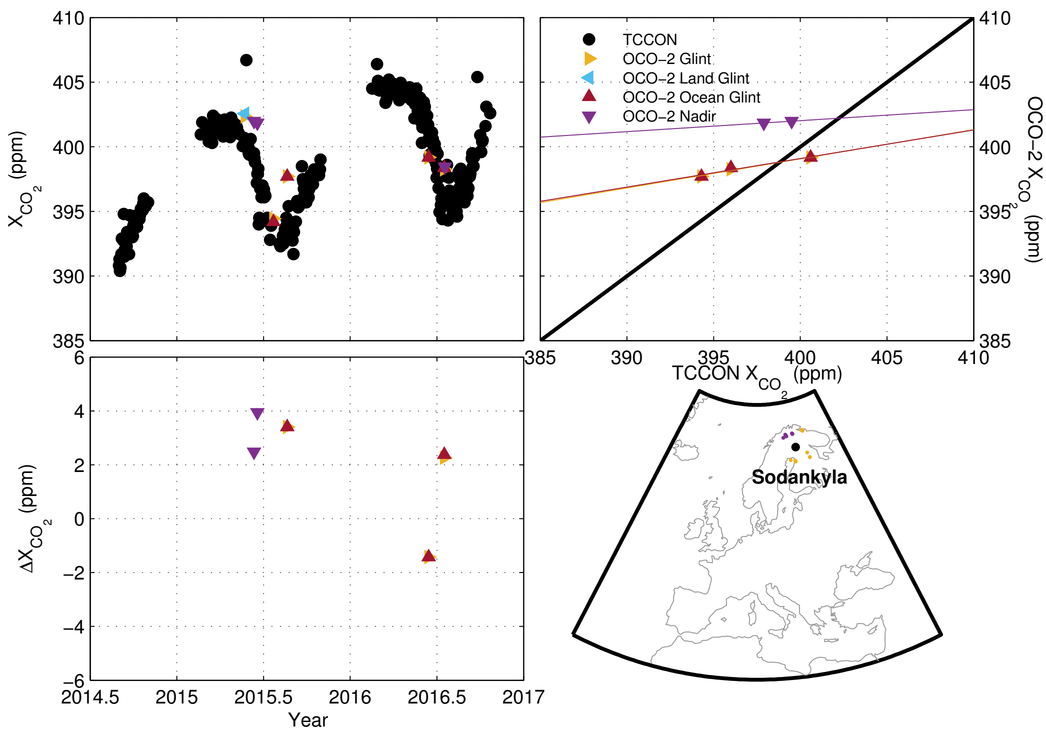

(b) Sodankylä. Note that the land glint OCO-2 measurement does not have a coincident TCCON measurement.

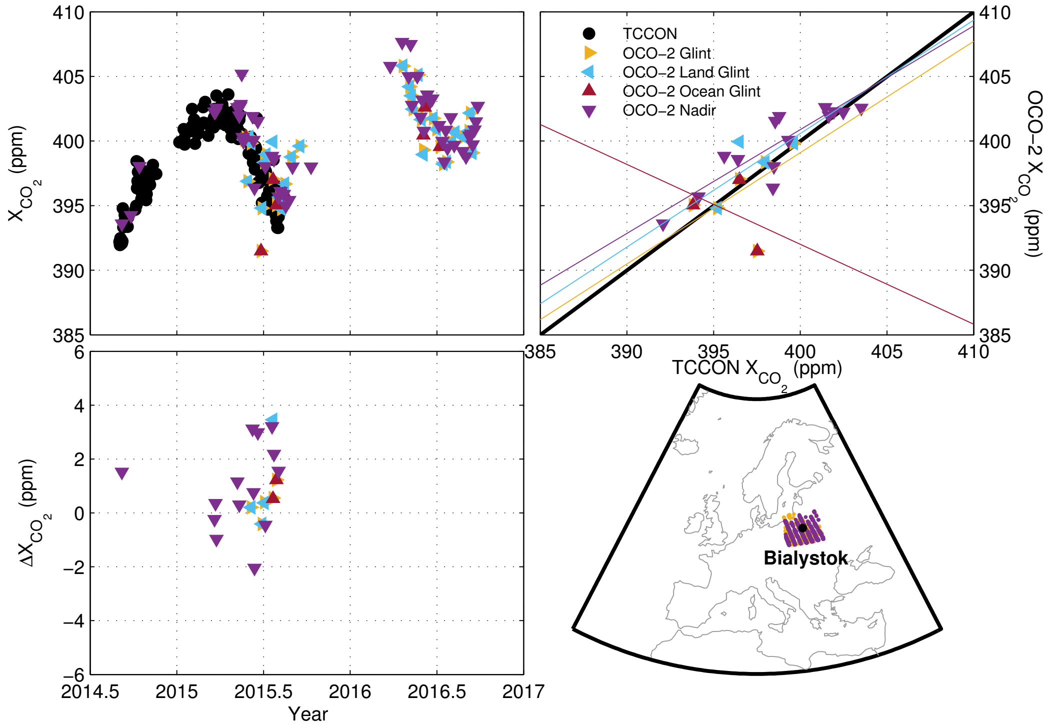

(c) Białystok

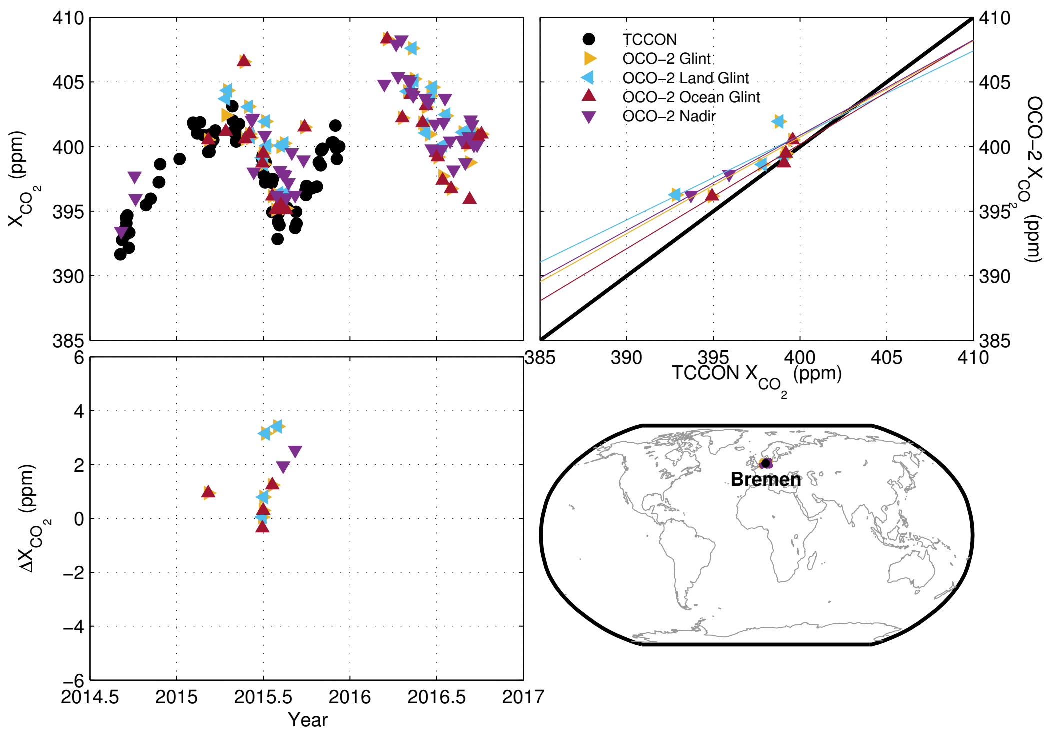

(d) Bremen

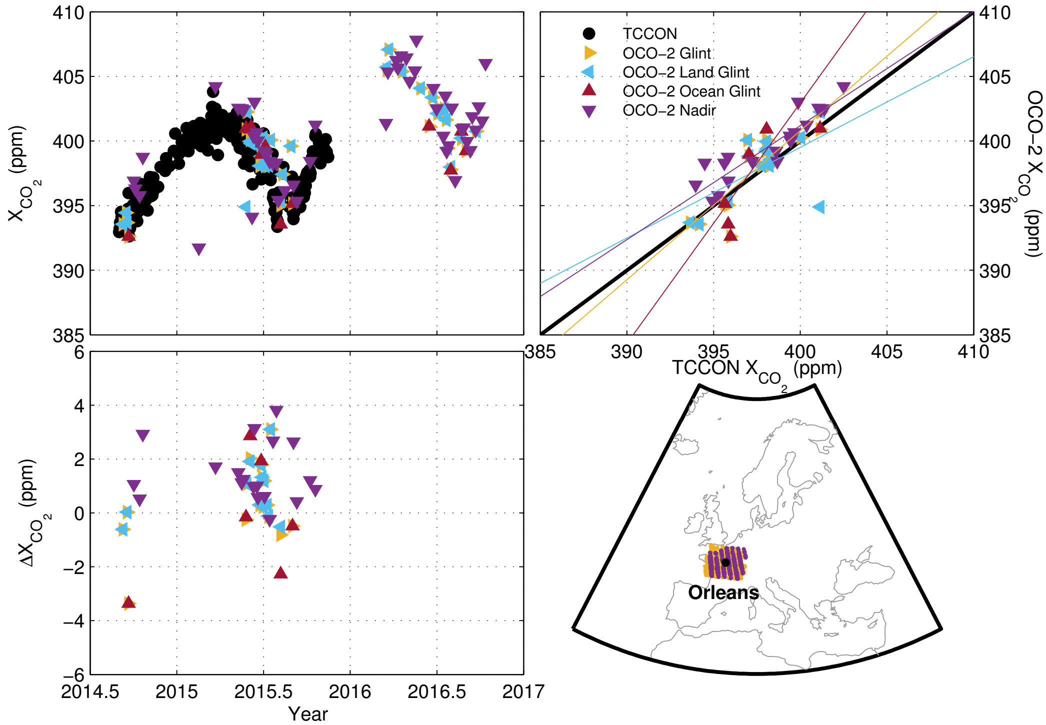

(e) Orléans

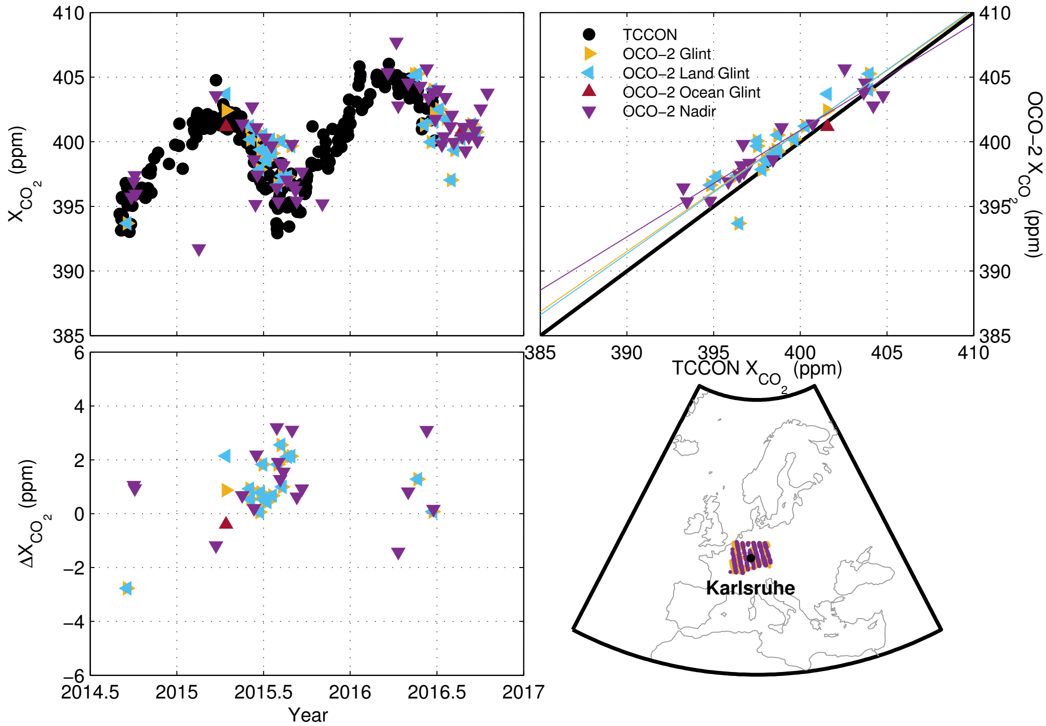

(f) Karlsruhe

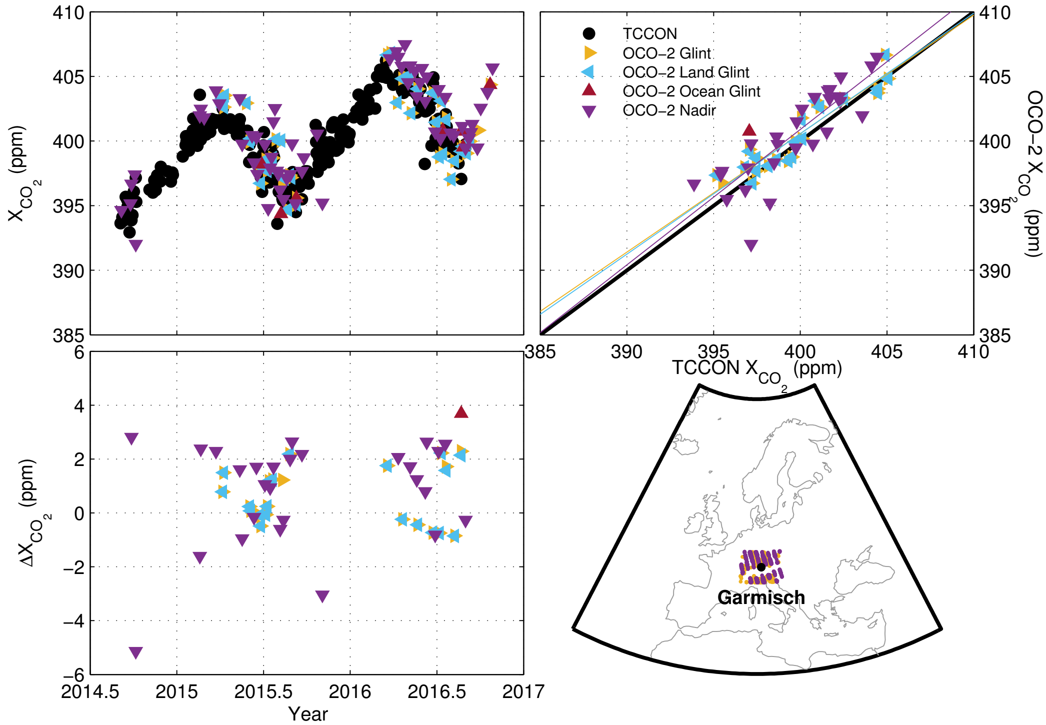

(g) Garmisch: Sussmann and Rettinger (2014)

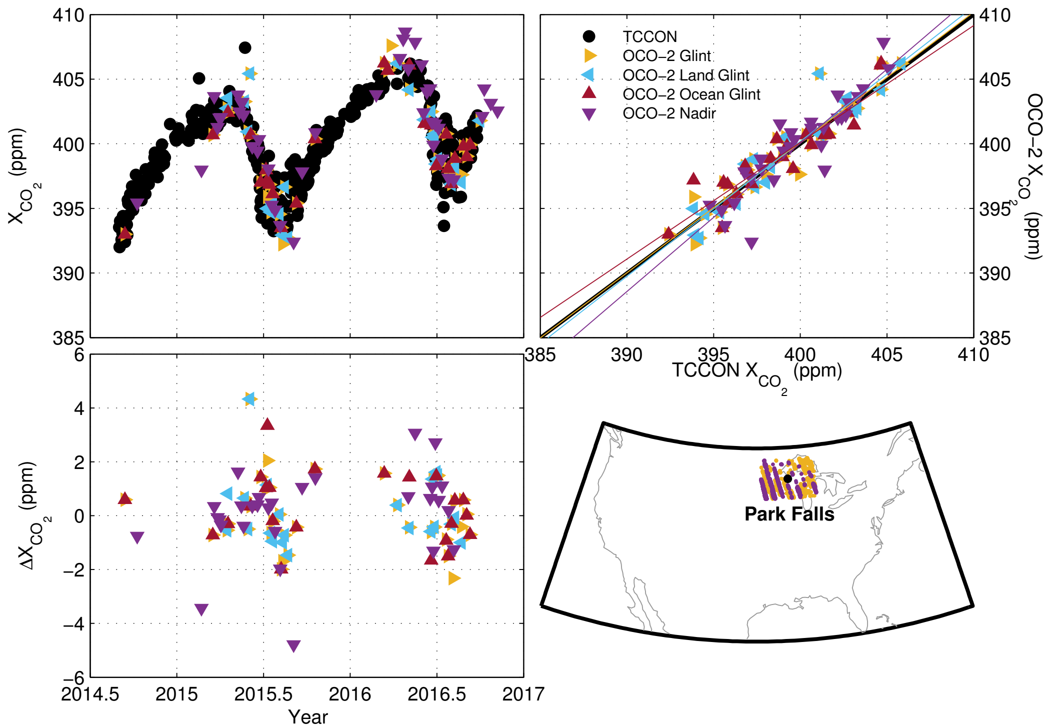

(h) Park Falls

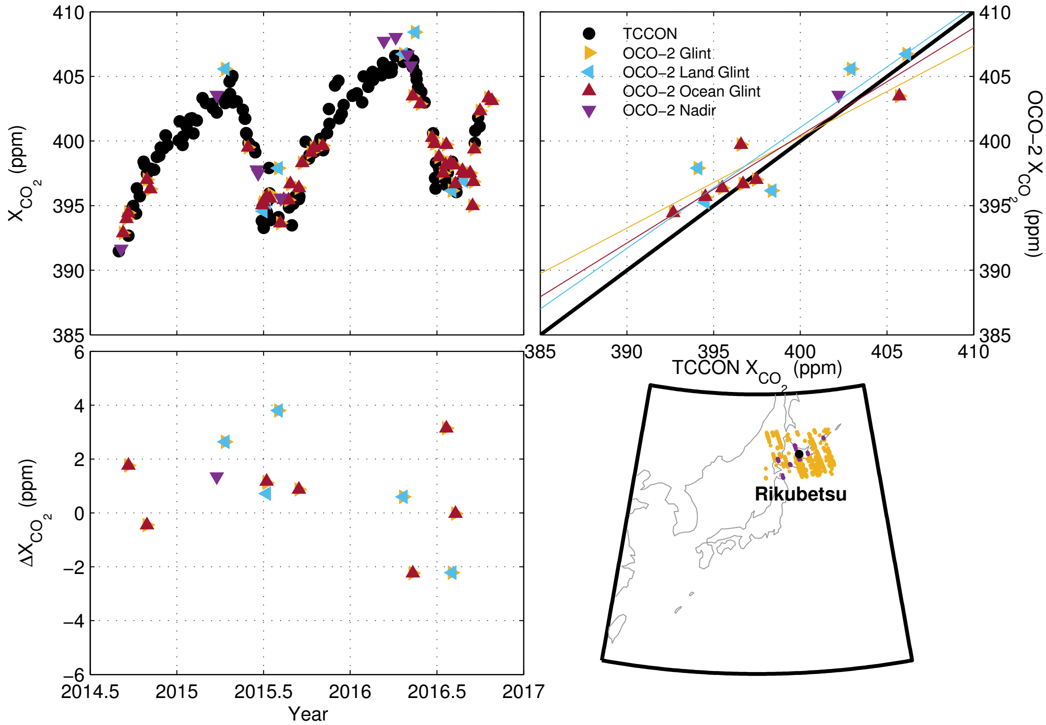

(i) Rikubetsu

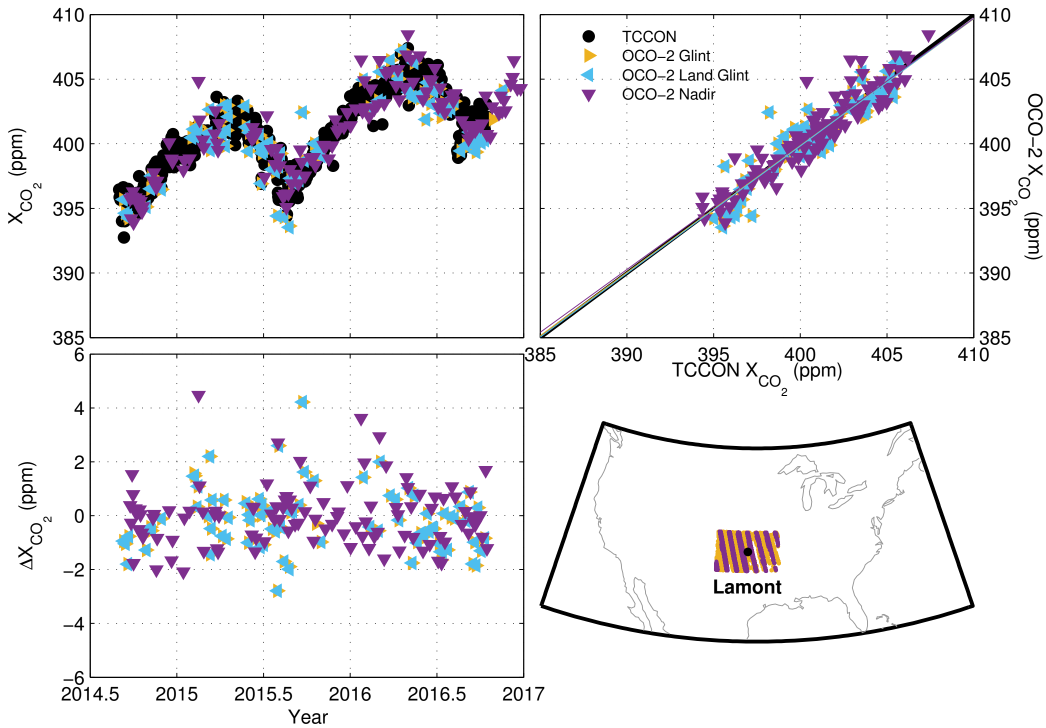

(j) Lamont

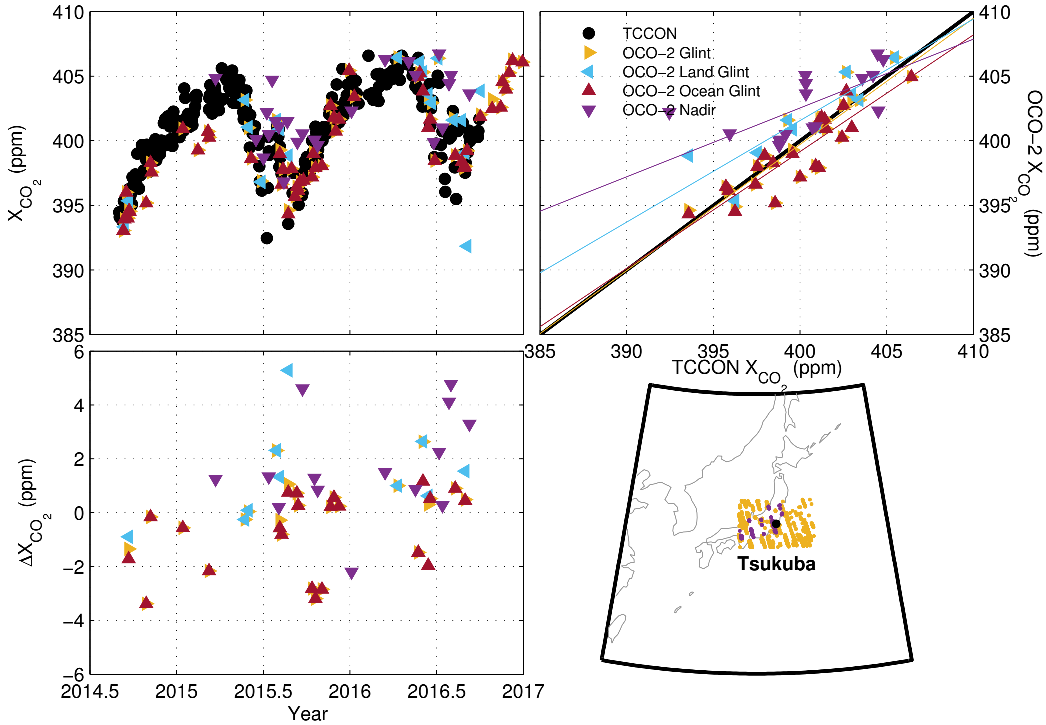

(k) Tsukuba

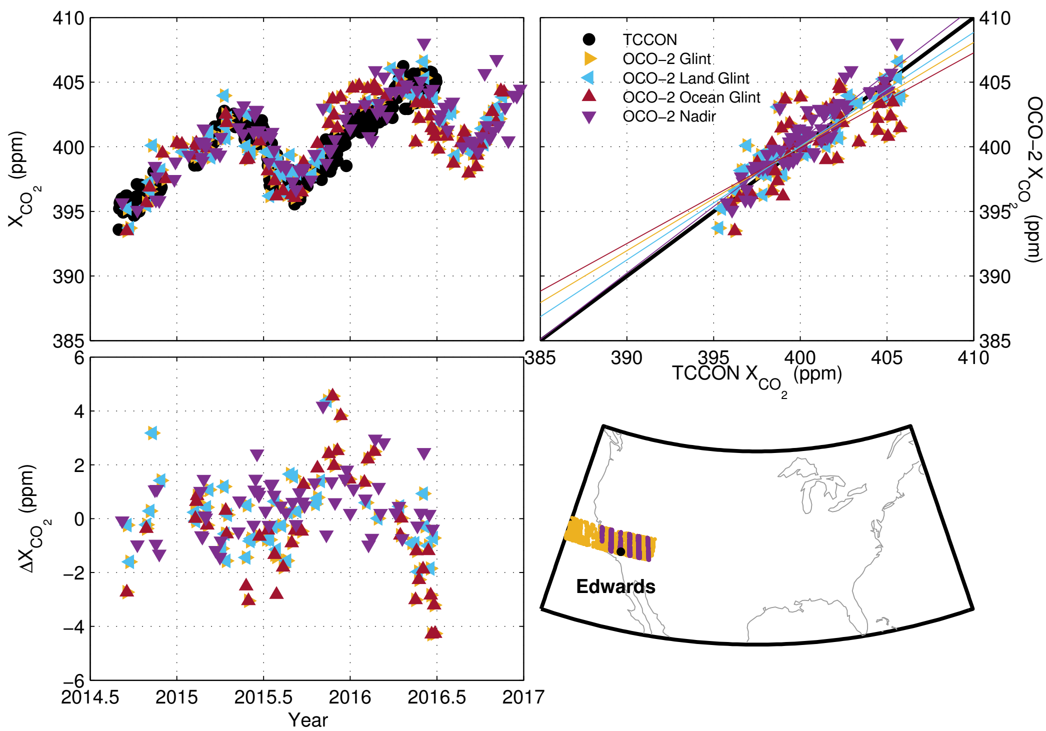

(l) Edwards

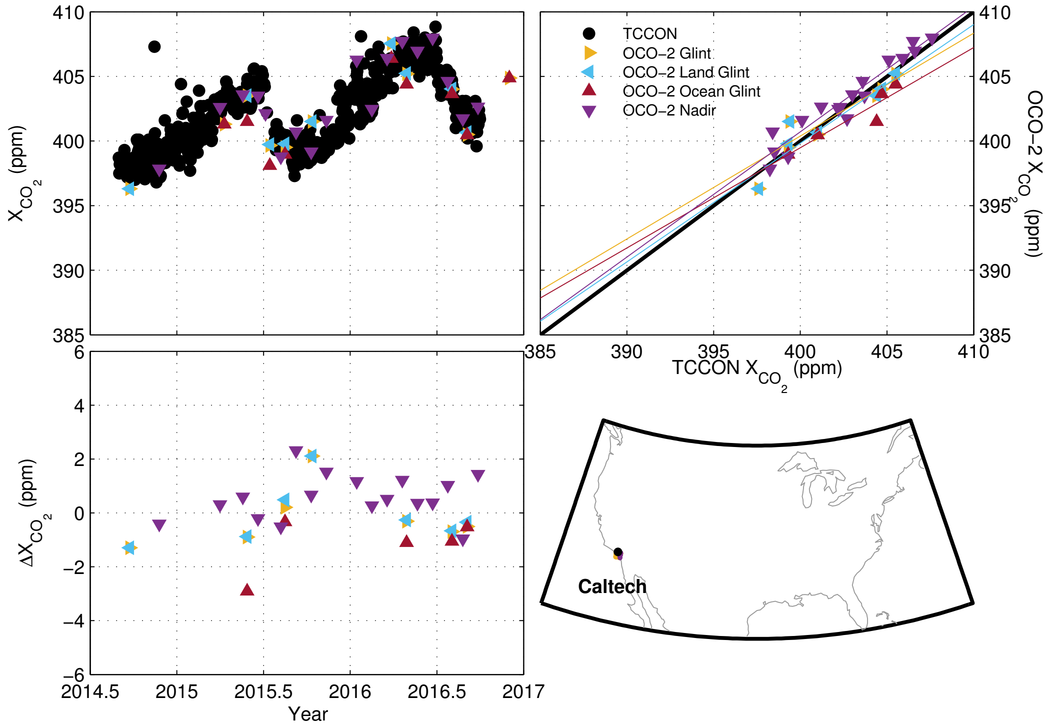

(m) Pasadena

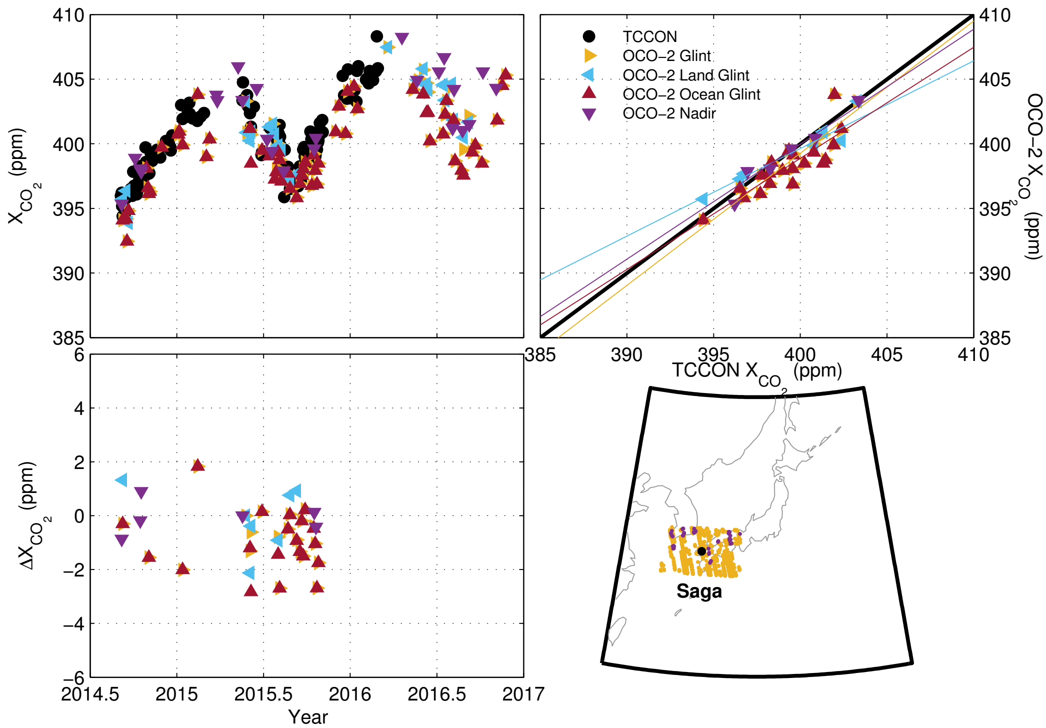

(n) Saga

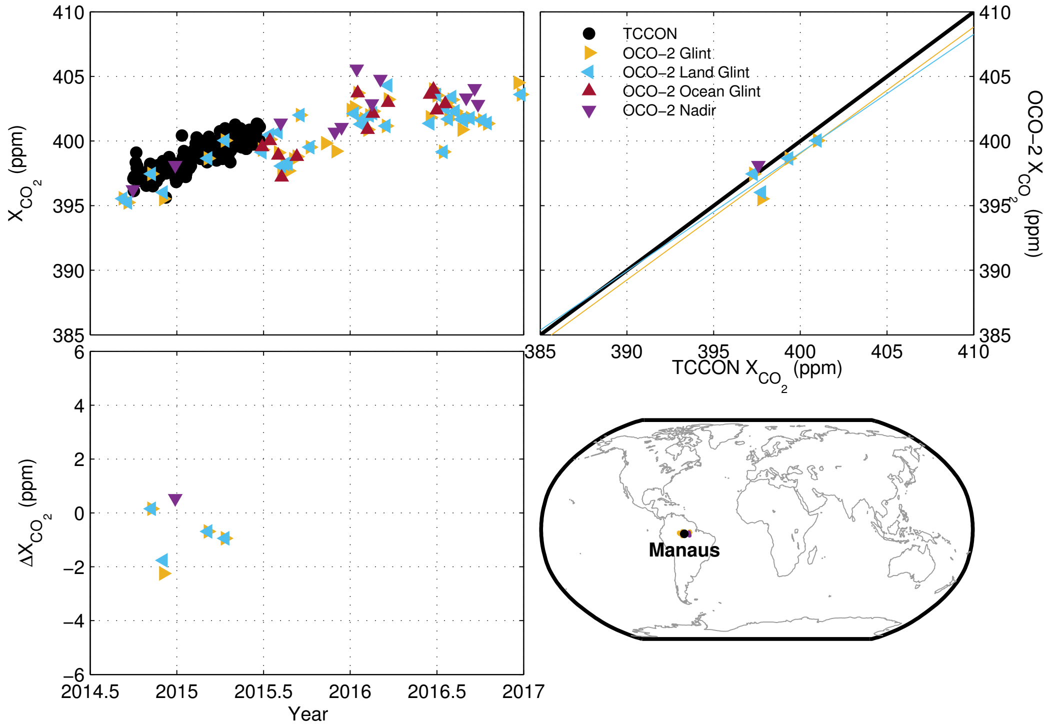

(o) Manaus

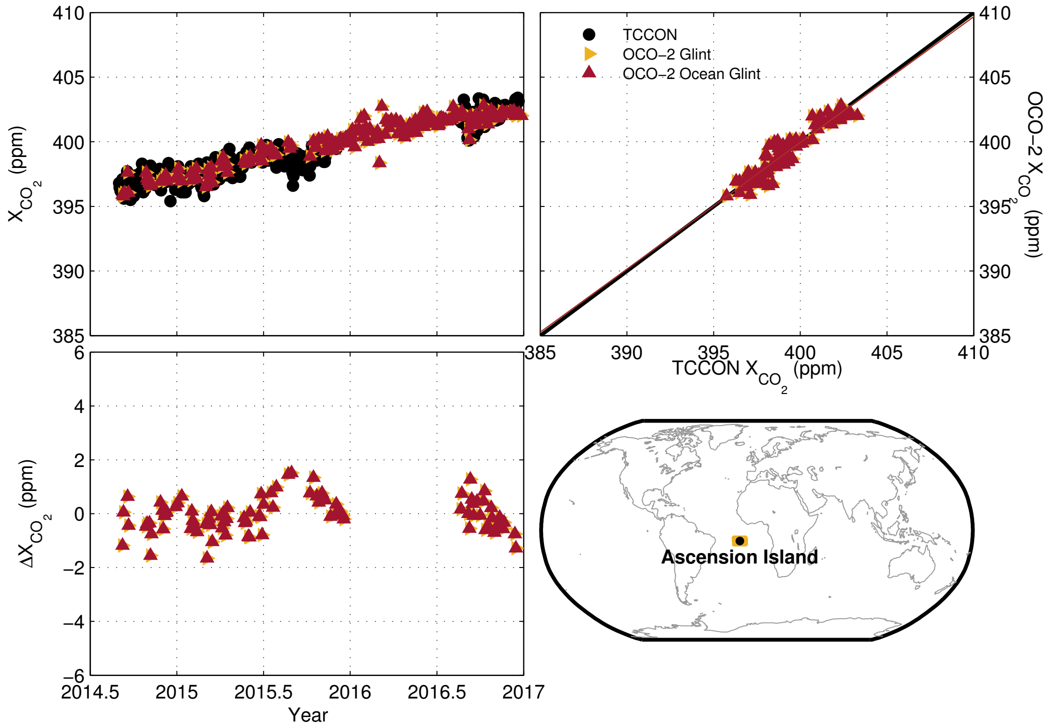

(p) Ascension

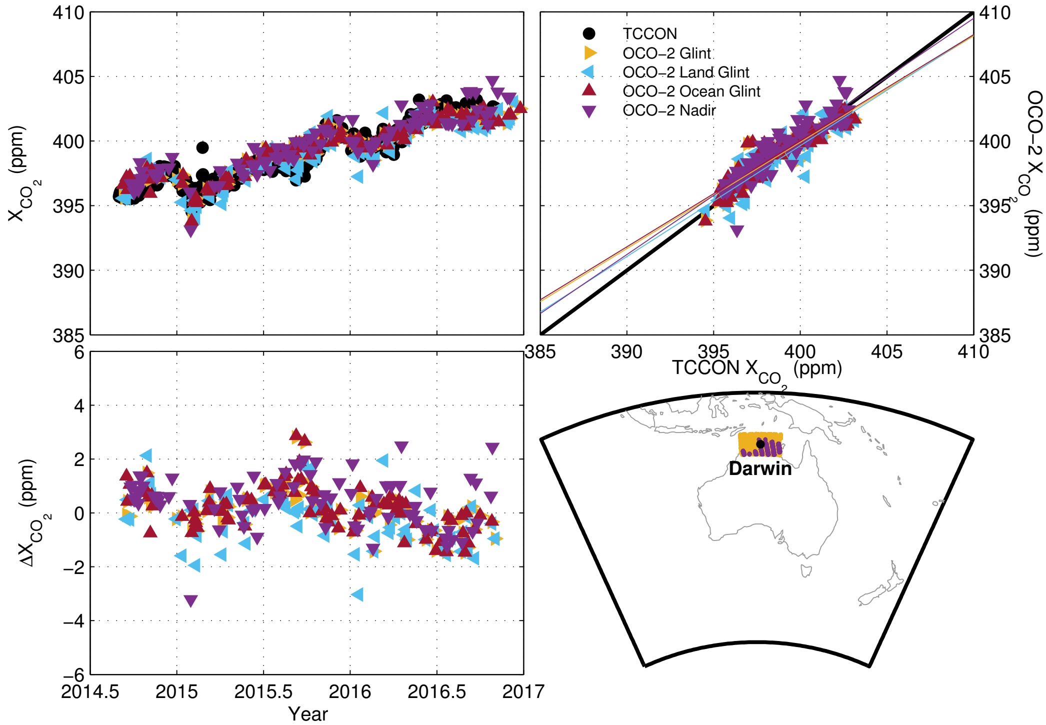

(q) Darwin

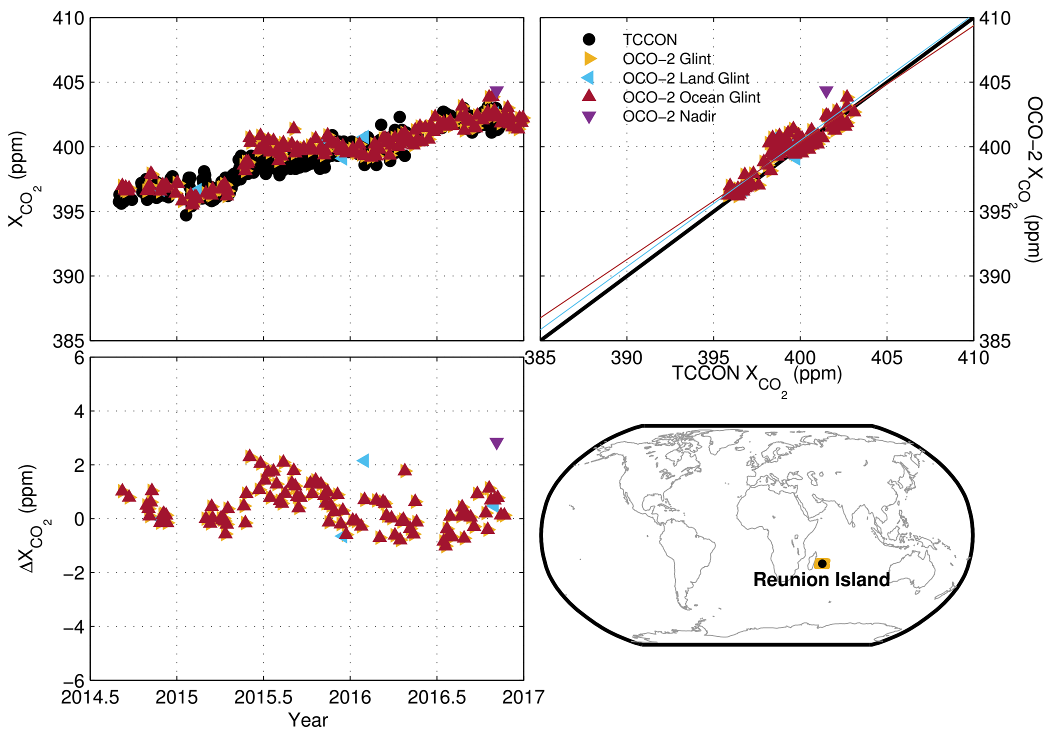

(r) Réunion Island

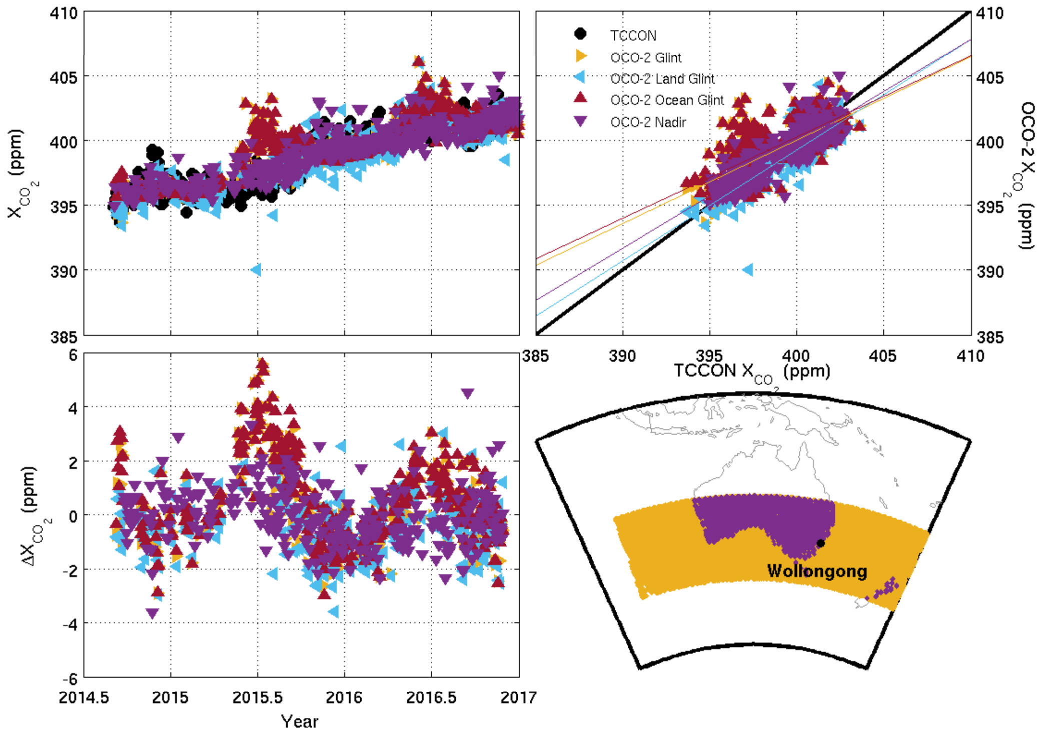

(s) Wollongong

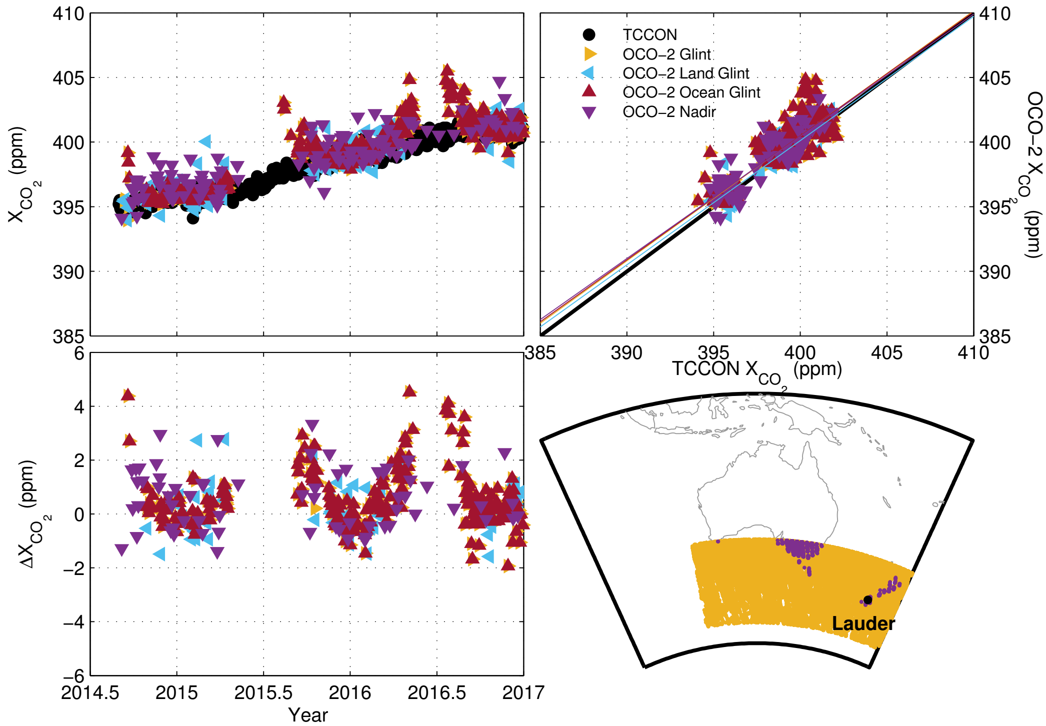

(t) Lauder

Figure A0: The top left panel of each plot (a–t) shows the time series of the TCCON daily medians (black circles), and the daily medians of the OCO-2 glint mode (gold triangles), split into land glint (blue triangles) and ocean glint (red triangles), and OCO-2 nadir mode (purple triangle). The bottom left panel shows the difference between the OCO-2 data and TCCON data as a function of time. The top right panel shows the one-to-one correspondence between the OCO-2 X_{CO_2} values and the TCCON values, and the best fit lines in the colours corresponding to the symbols. The one-to-one line is marked in black. The lower right panel shows the location of the TCCON station (black circle), and the locations of the OCO-2 data, showing glint-mode data in gold and nadir-mode data in purple. The lower right panel is intended to give a sense of the spatial coincidence criteria applied to the OCO-2 data for each TCCON station.

Table 1: Available targets. Those available only prior to July 2015 are marked with a natural symbol (♮). Those only available after July 2015 are marked with a sharp symbol (♯). Note that the Target Location (listed in degrees latitude, degrees longitude, and altitude above sea level (km)) may not be exactly centered on a TCCON site location. Targets without a corresponding TCCON station are marked with a flat symbol double dagger (♭‡) and are not discussed in this paper.

Target Name	Target Location (Lat, Lon, Alt)	Target Active Dates Target Active Dates	Data Reference Data Reference
Anmyeondo, South Korea ♯	36.624, 126.373, 0.006	July 2015 - Present	
Ascension Island	-7.947, -14.387, 0.165	July 2014 - Present	? Feist et al. (2014)
Białystok, Poland	53.196, 23.0758, 0.124	July 2014 - Present	? Deutscher et al. (2014)
Boulder, CO ♭ ‡	40.014 , -105.104 , 1.61	July 2015 - Present	
Bremen, Germany	53.104, 8.850, 0.004	July 2014 - Present	? Notholt et al. (2014)
Caltech, Pasadena, CA	34.123, -118.073, 0.157	July 2014 - Present	Wennberg et al. (2014c) Wennberg et al. (2014b)
ARM TWP - Darwin, Aus	-12.375, 130.917, 0.0049	July 2014 - Present	? Griffith et al. (2014a)
Edwards FRC, CA	34.958, -117.882, 0.699	July 2014 - Present	? Iraci et al. (2016)
Izaña, Tenerife, Spain	28.297, -16.518, 2.2317	July 2014 - Present	? Blumenstock et al. (2014)
Karlsruhe, Germany	49.100, 8.438, 0.11	July 2014 - Present	? Hase et al. (2014)
Eureka, Canada ♮	80.053, -86.417, 0.601	July 2014 - June 2015	? Strong et al. (2014)
SGP ARM Site, Lamont OK	36.604, -97.486, 0.3179	July 2014 - Present	? Wennberg et al. (2016)
Lauder, NZ	-45.002, 169.685, 0.384	July 2014 - Present	? Sherlock et al. (2014)
Libya ‡	28.550, 23.390, 0.108	June 2016 - Present	
Litchfield, Aus ‡	-17.151, 139.795, 0.233	June 2016 - Present	
Manaus, Brazil	-3.213, -60.598, 0.04877	July 2014 - June 2016	? Dubey et al. (2014)
Mexico City, Mexico ♭ ♯ ‡	19.429, -99.138, 2.239	July 2015 - Present	
Orléans, France	47.965, 2.113, 0.1308	July 2014 - Present	? Warneke et al. (2014)
Paris, France ♯	48.846, 2.356, 0.034	July 2015 - Present	? Te et al. (2014)
Park Falls, WI	45.945 , -90.273, 0.474	July 2014 - Present	? Wennberg et al. (2014a)
Fairbanks, Alaska ♭ ♯ ‡	64.859, -147.844, 0.501	July 2015 - Present	
Railroad Valley ♭ ‡	38.497, -115.690, 1.4359	July 2014 - Present	
Réunion Island	-21.049, 55.285, 0.504	July 2014 - Present	? De Mazière et al. (2014)
Rikubetsu, Japan	43.452, 143.700, 0.236	July 2015 - Present	? Morino et al. (2014b)
Rosemount, MN ♭ ♯ ‡	44.689, -93.027, 0.289	June 2016 - Present	
Saga, Japan	33.241, 130.288, 0.003	July 2015 - Present	? Kawakami et al. (2014)
São Paulo, Brazil ♭ ♯ ‡	-23.539, -46.634, 0.76	July 2015 - June 2016	
Shanghai, China ♭ ♯ ‡	31.22, 121.456, 0.12	July 2015 - June 2016	
Sodankylä, Finland	67.368, 26.633, 0.18	July 2014 - Present	? Kivi et al. (2014)
Tsukuba, Japan	36.051, 140.122 , 0.0277	July 2014 - Present	? Morino et al. (2014a)
Wollongong, Aus	-34.451, 150.855, 0.008	July 2014 - Present	?Griffith et al. (2014b)

Table 2: Filters applied to the target-mode OCO-2 data from the standard OCO-2 files (i.e., not the "lite" files). The parameters names listed below are written as they are in the standard L2 files. Parameters for which there is only one limit are marked with a '—'. The units are listed where applicable. The parameter "blended_albedo" is defined as $2.4 \times albedo\_o2\_fph - 1.13 \times albedo\_strong\_co2\_fph$. The tag "fph" are parameters from the full physics algorithm; "abp" are parameters from the A-band pre-processor algorithm designed for quick cloud screening; "idp" is the IMAP-DOAS pre-processor.

Parameter	Lower Bound	Upper Bound	Units	Description
surface_pressure_delta_abp	-4000	583	Pa	Surface pressure difference from the prior
retrieval_surface_roughness	—	26.50		Surface roughness
relative_residual_mean_square_weak_co2	—	0.00250		Spectral residuals in the weak CO_2 band
retrieval_zenith	—	40	°	Zenith angle of the retrieval
outcome_flag	—	2		Data quality flag
blended_albedo	—	0.8		Described in the table caption
h2o_ratio_idp	0.7	1.02		The ratio of water retrieved from the two CO_2 bands
co2_ratio_idp	0.995	1.025		The ratio of CO_2 between the two bands
surface_pressure_delta_fph	-5	10	hPa	Surface pressure difference from the prior
dof_co2_profile	1.8	—		Degrees of freedom for signal in the CO_2 profile
ice_aod	—	0.03		Ice aerosol optical depth extracted from the aerosol field
dust_aod	0.001	0.3		Dust aerosol optical depth extracted from the aerosol field
co2_grad_del	-70	70		The oscillation of the retrieved profile relative to the prior
sulfate_aod	0.4	—		Sulfate aerosol optical depth extracted from the aerosol field
albedo_weak_co2_fph	0.1	—		Weak CO_2 albedo
airmass	—	3.6		$\frac{1}{cos(solarzenith)} + \frac{1}{cos(retrievalzenith)}$
surface_type	Not 'Coxmunk'	Not 'Coxmunk'		Retain only soundings over land (pure Lambertian surfaces)

Table 3: Glint and nadir statistics for data filtered using Warn Levels ≤ 11 and the xco2_quality_flag = 0. The median bias (OCO-2 - TCCON) and its RMS, R^2 and number of daily median comparison points, or "coincidences" (N) are listed below for each TCCON station. If the number of coincidences is larger than 10, the results are marked in bold font to indicate that they are more statistically significant. The "Total" row is calculated by considering all the coincidences in the table independently.

	Land Glint				Ocean Glint					
~~**TCCON Site**~~	**Bias**	**RMS**	R^2	**N**	**Bias**	**RMS**	R^2	**N**	**Bias**	**RMS**
Eureka									~~0.10~~0.19	~~1.99~~2
~~**Sodankylä**~~**Sodankyla**					2.38	2.53	0.956	~~3.15~~3	3.21	3.29
~~**Białystok**~~**Bialystok**	0.29	1.75	0.485	4	0.53	3.57	~~0.181~~0.178	3	~~0.89~~**0.96**	~~1.83~~1
Bremen	1.98	2.36	0.665	4	~~0.63~~0.62	~~0.82~~0.81	~~0.903~~0.905	4	~~2.27~~2.25	~~2.29~~2
Karlsruhe	~~0.86~~**0.86**	~~1.55~~**1.49**	~~0.676~~**0.812**	~~16~~**18**					~~0.96~~**0.93**	~~1.69~~1
~~**Orléans**~~**Orleans**	~~0.29~~**0.29**	~~2.08~~**2.08**	~~0.369~~**0.387**	~~14~~**14**	~~-0.31~~-0.32	~~2.20~~2.18	~~0.256~~0.533	6	~~1.15~~**1.13**	~~1.82~~1
Garmisch	~~0.24~~**0.24**	~~1.00~~**1.19**	~~0.852~~**0.873**	~~11~~**20**					~~1.25~~**1.61**	~~2.13~~2
Park Falls	~~-0.50~~**-0.37**	~~1.44~~**1.27**	~~0.919~~**0.903**	~~13~~**22**	~~0.60~~**0.35**	~~1.42~~**1.28**	~~0.868~~**0.858**	~~13~~**23**	~~0.27~~**0.37**	~~1.55~~1
Rikubetsu	~~2.64~~0.72	~~2.70~~2.33	~~0.917~~0.825	~~3~~5	~~1.02~~0.87	~~1.10~~1.70	~~0.932~~0.813	~~4~~7		
Lamont	~~-0.20~~**-0.30**	~~1.23~~**1.16**	~~0.854~~**0.865**	~~52~~**78**					~~-0.13~~**-0.03**	~~1.18~~1
Tsukuba	~~0.71~~1.17	~~2.47~~2.16	~~0.530~~0.765	~~6~~10	~~-0.56~~**-0.36**	~~1.79~~**1.61**	~~0.698~~**0.772**	~~16~~**22**	~~1.34~~**1.34**	~~3.80~~3
Edwards	~~-0.08~~**-0.09**	~~1.27~~**1.25**	~~0.732~~**0.842**	~~35~~**45**	~~-0.13~~**-0.45**	~~1.97~~**2.16**	~~0.579~~**0.529**	~~28~~**40**	~~0.34~~**0.48**	~~1.17~~1
Pasadena	~~-0.26~~-0.34	~~1.20~~1.05	~~0.856~~0.867	~~5~~7	~~-1.08~~-1.05	~~1.79~~1.49	~~0.851~~0.865	~~3~~5	~~0.49~~**0.51**	~~0.99~~0
Saga	0.00	1.11	~~0.916~~0.915	7	~~-1.12~~**-1.12**	~~1.50~~**1.51**	~~0.715~~**0.716**	~~20~~**20**	~~-0.18~~-0.09	~~0.62~~0
Manaus	-0.82	1.06	0.795	4						
Ascension Island					~~-0.09~~**-0.09**	~~0.63~~**0.62**	~~0.736~~**0.899**	~~66~~**90**		
Reunion Island	0.47	1.06	0.775	5	**0.30**	**0.81**	**0.873**	**99**		
Darwin	~~0.10~~**-0.16**	~~0.96~~**0.97**	**0.843**	**70**	**0.14**	**0.84**	**0.881**	**86**	**0.51**	**1.03**
Wollongong	**-0.67**	**1.32**	**0.733**	**253**	**0.20**	**1.70**	**0.487**	**366**	**-0.12**	**1.04**
Lauder	**0.09**	**0.96**	**0.829**	**54**	**0.35**	**1.18**	**0.782**	**235**	**0.63**	**1.25**
Total	**-0.27**	**1.29**	**0.787**	**620**	**0.17**	**1.41**	**0.664**	**1011**	**0.22**	**1.31**

Table 4: Glint and nadir statistics for data filtered using Warn Levels ≤ 15 and the xco2_quality_flag = 0. The median bias (OCO-2 - TCCON) and its RMS, R^2 and number of daily median comparison points, or "coincidences" (N) are listed below for each TCCON station. If the number of coincidences is larger than 10, the results are marked in bold font to indicate that they are more statistically significant. The "Total" row is calculated by considering all the coincidences in the table independently. In general, the RMS values are equal or larger than those in Table 3 despite the fact that the number of coincidences is larger.

	Land Glint				Ocean Glint				
TCCON Site	**Bias**	**RMS**	R^2	**N**	**Bias**	**RMS**	R^2	**N**	**Bias**
Eureka	~~0.676~~	~~46~~	~~0.40~~						-0.19
Sodankyla	~~0.58~~2.24	~~1.04~~2.46	~~0.711~~0.973	~~56~~4	1.52	2.85	0.417	10	2.60
~~**Réunion Island**~~**Bialystok**	~~0.27~~1.51	2.44	0.546	9	0.60	1.12	0.996	3	**1.29**
Bremen	1.36	2.26	0.800	10	1.36	1.45	0.905	6	2.04
Karlsruhe	**1.69**	**2.22**	**0.815**	**27**	1.60	2.28	0.661	4	**1.48**
Orleans	**0.92**	**2.23**	**0.601**	**21**	0.09	1.60	0.681	9	**1.26**
Garmisch	**1.14**	**1.76**	**0.834**	**28**	-0.72	2.55	0.441	4	**1.52**
Park Falls	**0.36**	**1.62**	**0.845**	**42**	**0.50**	**1.67**	**0.798**	**38**	**0.54**
Rikubetsu	1.37	2.25	0.907	6	**0.48**	**1.57**	**0.913**	**12**	0.32
Lamont	**0.01**	**1.33**	**0.827**	**98**	0.18	0.74	0.969	5	**-0.07**
Tsukuba	**1.33**	**2.01**	**0.819**	**12**	**-0.25**	**1.45**	**0.782**	**31**	**2.31**
Edwards	**0.18**	**1.71**	**0.711**	**54**	**-0.18**	**1.99**	**0.582**	**47**	**0.44**
Pasadena	-0.22	3.37	0.169	10	-0.86	1.16	~~0.582~~0.940	5	**0.39**
Saga	**0.46**	**1.34**	**0.761**	**14**	**-1.03**	**1.33**	**0.912**	**25**	**0.30**
Manaus	**0.01**	**1.54**	**0.512**	**11**	-0.39	0.51	1.000	2	0.98
Ascension Island	~~0.50~~	~~0.90~~	~~0.824~~	~~63~~	**0.03**	**0.67**	**0.893**	**92**	
Reunion Island	0.47	1.58	0.593	5	**0.41**	**0.81**	**0.893**	**100**	1.51
Darwin	**-0.12**	**0.88**	**0.871**	**81**	**0.29**	**0.84**	**0.890**	**87**	**0.57**
Wollongong	~~-0.69~~**-0.52**	~~1.40~~**1.34**	~~0.638~~**0.670**	~~154~~**287**	~~0.18~~**0.26**	~~2.01~~**1.65**	~~0.183~~**0.517**	~~220~~**367**	~~0.03~~**-0.11**
Lauder	~~0.03~~**0.46**	~~0.98~~**1.91**	~~0.731~~**0.547**	~~41~~**84**	~~0.27~~**0.45**	~~0.97~~**1.30**	~~0.749~~**0.768**	~~136~~**242**	~~0.69~~**1.02**
Total	~~-0.21~~**0.07**	~~1.36~~**1.59**	~~0.716~~**0.704**	~~419~~**804**	~~0.19~~**0.26**	~~1.51~~**1.42**	~~0.501~~**0.694**	~~644~~**1089**	~~0.29~~**0.36**

Table 5: ~~Glint~~Bias corrected glint, nadir and target relationships with TCCON. The slope and its uncertainty, R^2 and number of daily median comparison points (N) are listed below for each OCO-2 viewing mode. The uncertainties on the slopes are the standard deviation of the slopes computed through bootstrapping. The values for ocean glint data with and without the southern hemisphere winter data are included on separate rows. Note that the ~~land glint, ocean glint and nadir~~ slopes are computed after the global bias has been removed from the data and the residual footprint corrections have been applied. The ~~global bias is determined by~~ glint and nadir data are filtered with warn level ≤ 11 and xco2 quality flag $= 0$; the ~~target~~ target-mode data ~~value listed in~~ are filtered using the ~~table~~filters described in Table 2.

	slope	R^2	**N**
Land Glint	~~0.9074~~0.9035±0.02	~~0.72~~0.79	~~419~~620
Ocean Glint	~~0.7167~~0.7921±~~0.03~~0.02	~~0.50~~0.66	~~644~~1011
Ocean Glint Excluding SH Winter	~~0.8164~~0.8528±~~0.03~~0.02	~~0.71~~0.76	~~501~~743
Nadir	~~0.8690~~0.8996±~~0.03~~0.02	~~0.75~~0.80	~~555~~780
Target	~~0.9975~~1.0007±~~0.04~~0.03	~~0.81~~0.86	~~106~~123